



ANALYSIS OF FIRING RATE AND CORRELATION OF SPIKE TRAINS
FROM A BRAIN NETWORK MODEL WITH CLUSTERS

Conrado Catarcione Pinto

Dissertação de Mestrado apresentada ao Programa de Pós-graduação em Engenharia de Sistemas e Computação, COPPE, da Universidade Federal do Rio de Janeiro, como parte dos requisitos necessários à obtenção do título de Mestre em Engenharia de Sistemas e Computação.

Orientadores: Daniel Ratton Figueiredo
Guilherme Ost de Aguiar

Rio de Janeiro
Fevereiro de 2025

ANALYSIS OF FIRING RATE AND CORRELATION OF SPIKE TRAINS
FROM A BRAIN NETWORK MODEL WITH CLUSTERS

Conrado Catarcione Pinto

DISSERTAÇÃO SUBMETIDA AO CORPO DOCENTE DO INSTITUTO
ALBERTO LUIZ COIMBRA DE PÓS-GRADUAÇÃO E PESQUISA DE
ENGENHARIA DA UNIVERSIDADE FEDERAL DO RIO DE JANEIRO COMO
PARTE DOS REQUISITOS NECESSÁRIOS PARA A OBTENÇÃO DO GRAU DE
MESTRE EM CIÊNCIAS EM ENGENHARIA DE SISTEMAS E COMPUTAÇÃO.

Orientadores: Daniel Ratton Figueiredo
Guilherme Ost de Aguiar

Aprovada por: Prof. Daniel Ratton Figueiredo
Prof. Guilherme Ost de Aguiar
Prof. Franklin de Lima Marquezino
Prof. Maximilien Drevetton

RIO DE JANEIRO, RJ – BRASIL
FEVEREIRO DE 2025

Pinto, Conrado Catarcione

Analysis of Firing Rate and Correlation of Spike Trains from a Brain Network Model with Clusters/Conrado Catarcione Pinto. – Rio de Janeiro: UFRJ/COPPE, 2025.

IX, 46 p.: il.; 29, 7cm.

Orientadores: Daniel Ratton Figueiredo

Guilherme Ost de Aguiar

Dissertação (mestrado) – UFRJ/COPPE/Programa de Engenharia de Sistemas e Computação, 2025.

Referências Bibliográficas: p. 38 – 40.

1. Brain Networks. 2. Spike Train Analysis. 3. Correlation Analysis. I. Figueiredo, Daniel Ratton *et al.* II. Universidade Federal do Rio de Janeiro, COPPE, Programa de Engenharia de Sistemas e Computação. III. Título.

*Para meu irmão, que me
ensinou a não ser sozinho.*

Agradecimentos

Agradeço aos meus pais, Sandra e Wellington, e ao meu irmão, Bernardo, por todo o apoio durante a minha vida.

Ao Professor Daniel, por me aceitar em um momento de dúvidas e por ter me guiado ao meu futuro. Aos Professores Guilherme e Giulio, por me conduzirem em um mundo probabilístico, e ao Thiago, com quem dividi esse desafio.

Agradeço ao Rodrigo, ao Fabio e ao Davi pela companhia durante esses anos de muito aprendizado. Aos professores do programa, como Botler, Laura e Celina, cujas didáticas excepcionais me motivaram e me inspiraram a buscar a excelência. E a todos os funcionários do PESC, por removerem obstáculos nessa trajetória.

Ao Rafa, ao Lucca e à Olivia, pela longa amizade.

E agradeço à Amanda, que, com seu exemplo diário, me inspira a ser uma pessoa melhor.

Resumo da Dissertação apresentada à COPPE/UFRJ como parte dos requisitos necessários para a obtenção do grau de Mestre em Ciências (M.Sc.)

ANÁLISE DE TAXA DE DISPAROS E CORRELAÇÃO DE SEQUÊNCIAS DE DISPAROS DE UM MODELO DE REDE CEREBRAL COM COMUNIDADES

Conrado Catarcione Pinto

Fevereiro/2025

Orientadores: Daniel Ratton Figueiredo
Guilherme Ost de Aguiar

Programa: Engenharia de Sistemas e Computação

Compreender as dinâmicas complexas do cérebro humano continua a ser um dos maiores desafios da neurociência moderna. Uma das abstrações-chave usadas para modelar a atividade cerebral é a rede estrutural do cérebro, que conceitualiza os neurônios como nós e as sinapses como arestas direcionadas e ponderadas. No entanto, essas arestas não são diretamente observáveis; em vez disso, a atividade neuronal é tipicamente medida utilizando sondas que registram simultaneamente as sequências de disparo de centenas de neurônios. Embora as correlações empíricas entre essas sequências tenham sido usadas para reconstruir a rede estrutural subjacente, há uma compreensão limitada sobre a natureza dessas correlações e seus efeitos na reconstrução da rede e no agrupamento neuronal. Este trabalho apresenta uma análise matemática rigorosa da taxa média de disparos e das covariâncias (e correlações) entre trens de disparo sob um modelo probabilístico linear simples para a dinâmica de atividade neuronal em um modelo de rede com duas comunidades. Derivamos expressões analíticas para as covariâncias síncronas e de um atraso, demonstrando suas dependências em relação aos parâmetros do modelo. Além disso, assumindo que a rede é gerada pelo Stochastic Block Model (incorporando pesos nas arestas) com duas comunidades, fornecemos a taxa média assintótica de disparo e uma expressão para a covariância assintótica dos disparos síncronos no caso de tamanhos idênticos das comunidades. De maneira notável, identificamos apenas dois valores assintóticos distintos para a taxa média de disparo, relacionados à filiação comunitária de cada neurônio; também encontramos apenas dois valores distintos para a covariância assintótica, correspondentes a pares intra-comunidade e inter-comunidade, o que oferece valiosas percepções sobre o agrupamento da rede.

Abstract of Dissertation presented to COPPE/UFRJ as a partial fulfillment of the requirements for the degree of Master of Science (M.Sc.)

ANALYSIS OF FIRING RATE AND CORRELATION OF SPIKE TRAINS
FROM A BRAIN NETWORK MODEL WITH CLUSTERS

Conrado Catarcione Pinto

February/2025

Advisors: Daniel Ratton Figueiredo
Guilherme Ost de Aguiar

Department: Systems Engineering and Computer Science

Understanding the intricate dynamics of the human brain remains one of the most profound challenges in modern neuroscience. One of the key abstractions used to model brain activity is the structural brain network, which conceptualizes neurons as nodes and synapses as directed and weighted edges. However, these edges are not directly observable; instead, neuronal activity is typically measured using probes that simultaneously record the spike trains of hundreds of neurons. Although empirical correlations between these spike trains have been used to reconstruct the underlying structural network, there is limited insight into the nature of these correlations and their effects on network reconstruction and neuronal clustering. This work presents a rigorous mathematical analysis of the average firing rate and pairwise spike train covariances (and correlations) under a simple linear probabilistic model for neuronal firing dynamics in a network model with two clusters. We derive analytical expressions for the synchronous and the one-lagged covariances, demonstrating their dependence on key model parameters. Additionally, assuming the network is generated by the Stochastic Block Model (incorporating edge weights) with two clusters, we provide the asymptotic mean firing rate and an expression for the asymptotic pairwise synchronous firing covariance in the case of identical cluster sizes, including an error bound. Remarkably, we identify only two distinct asymptotic values for the firing mean, related to the cluster membership of each neuron; we also have only two distinct values for the asymptotic covariance, corresponding to intra-cluster and inter-cluster pairs, which offers valuable insights into the organization of the neuronal network as well as network clustering.

Contents

List of Figures	ix
1 Introduction	1
2 Concepts and Related Work	4
2.1 Neuroscience Principles	4
2.2 Random Graphs and Communities	6
2.3 Markov Chains	9
2.4 Related Work	9
3 Neurons Firing Model with Communities (NFC) on a Fixed Environment	12
3.1 Modelling Neuronal Activity	12
3.2 Theoretical Results	14
3.3 Empirical and Numerical Analyses	21
4 Neurons Firing Model with Communities (NFC) on a Random Environment	27
4.1 Mean-field Approximations	28
4.2 Validation of Mean-Field Approximations Against Theoretical Results	34
5 Conclusion	36
5.1 Future Work	37
References	38
A Rigorous Proofs	41

List of Figures

2.1	Neuron's anatomy	5
2.2	The bridges of Königsberg	7
2.3	Stochastic Block Model	8
3.1	Example graph	16
3.2	Firing mean CDF	22
3.3	Synchronous firing covariance CDF	23
3.4	One-lagged firing covariance CDF	24
3.5	Covariance heatmaps	25
3.6	Mean absolute error for firing rate	26
3.7	Mean absolute error for correlations	26
4.1	Asymptotic mean firing absolute error	35
4.2	Asymptotic synchronous firing covariance absolute error	35

Chapter 1

Introduction

The connectionist view of neuroscience has proven, over the last decades, to be fundamental for understanding the functioning of our most fascinating organ: the brain. Our ability to think, feel, move, and perform countless other functions is not entirely decipherable when studying neurons in isolation; it is only by examining the broader picture - monitoring the patterns of connections between neurons and the pathways of neuronal signals - that we can gain profound insights into the brain's most complex tasks, such as cognition and memory.

The challenge emerges from the brain's incredible size and interconnected complexity (approximately 86 billion neurons) and from the difficulty of observing its rapid, multifaceted activities (SEGUIN *et al.*, 2023; LYNN and BASSETT, 2019; HERCULANO-HOUZEL, 2009).

Neurons communicate through electrical signals, known as action potentials, which are generated when a cell's electrical potential exceeds a specific threshold. When a neuron fires, these signals travel along the axons and are then transmitted to other cells through chemical or electrical synapses, influencing their activity and prompting them to fire, creating a cascading effect. This dynamic is highly sensitive to the structure of the connections between neurons in the system, making it crucial to examine the collective behaviour of neurons (KANDEL *et al.*, 2000).

Networks, or graphs, are particularly well-suited for modelling the underlying structure of these interactions, allowing us to study dynamics influenced by neuronal connections. Furthermore, many real-world networks display an organisational pattern of communities, i.e., their nodes are divided into blocks, with a higher density of connections between nodes within the same block than between nodes in different blocks. This phenomenon is also evident in the brain's neuronal network, which is organised into functional modules.

Two main network representations are commonly considered when investigating brain activity: structural and functional networks (SEGUIN *et al.*, 2023; LYNN and BASSETT, 2019; SPORNS and BETZEL, 2016). The former models individual

neurons as nodes and synapses as directed and weighted edges, while the latter models brain regions as nodes, with edges representing interactions between regions under specific stimuli.

Inferring edges in structural and functional networks is challenging, as this typically requires interpreting data from noisy measurement techniques (DONNER *et al.*, 2024; REN *et al.*, 2020). Two common approaches involve measuring the activity of hundreds of neurons simultaneously using probes or employing imaging devices to measure chemical flows across millions of tiny brain regions. The result is often a collection of synchronised time series that track the evolution of specific neuronal quantities over time. In the case of the first approach, raw neuronal measurements are typically converted into spike trains, a discrete time series that records whether a neuron fires, yielding a binary sequence for each neuron.

In this context, a natural and fundamental problem is reconstructing the structural or functional network using these time series. While this task remains a significant hurdle, recent research has introduced various approaches, each based on different assumptions and methodologies, to address this problem (DONNER *et al.*, 2024; KORHONEN *et al.*, 2021; KOBAYASHI *et al.*, 2019; ENDO *et al.*, 2021).

A cornerstone technique in network reconstruction is correlation analysis. Intuitively, a strong correlation between two distinct time series suggests a potential interaction, thereby indicating the presence of a connection. A straightforward approach might apply a threshold to pairwise correlations to infer the presence of an edge, while more advanced methods often take a Bayesian approach to modelling these interactions. However, a fundamental question arises: Can these correlations be quantified? A rigorous exploration of this question represents one of the central contributions of this work.

Problem Statement and Contributions

Consider a graph G , directed and weighted, representing a given structural brain network. Positive and negative weights correspond to excitatory and inhibitory synapses among neurons, respectively. Assume that the nodes belong to one of two communities (clusters), and the edge weights take one of two possible values, depending on whether the respective nodes are within the same community or belong to different communities. It is important to note that G can either be a fixed graph or a sample from a random graph model, such as the Stochastic Block Model (SBM), extended to generate directed edges and both positive and negative edge weights accordingly.

Consider a discrete-time stochastic firing process, where $p_{G,i}(x)$ is the probability that neuron i fires at time t given vector x representing the firing pattern of all neurons at time $t - 1$. The probability $p_{G,i}(x)$ is modelled as a linear function that

accounts for the state of the in-neighbours of i at time $t - 1$ and their respective edge weights. This stochastic process can be represented as an ergodic Markov chain on the state space of all firing patterns (further details are provided in Section 3.1).

Main Theoretical Contributions:

- For any suitable graph G , we provide an analytical expression for the mean firing rate (or firing probability) of each neuron (see Theorem 3.1).
- For any suitable graph G , we derive an analytical expression for the synchronous firing covariance for any pair of neurons (see Theorem 3.2). This result can be extended to obtain an expression for the one-lagged firing covariance (see Proposition 3.3).
- If G is a suitable sample from the extended SBM, we provide an analytical expression for each neuron's asymptotic mean firing rate (or firing probability). Interestingly, there are at most two possible limiting values, related to the neuron's community membership (see Section 4.1).
- If G is a suitable sample from the extended SBM with identical community sizes, we provide an analytical expression for the asymptotic synchronous firing covariance for any pair of neurons. Remarkably, this scales as a constant over N , where the constant assumes at most two possible limiting values, one for neurons within the same community and one for neurons belonging to different communities (see Section 4.1).

Organisation

The remainder of this dissertation is organised as follows. Chapter 2 presents some fundamental concepts for understanding the following ideas derived in this text. Chapter 3 starts by presenting the modelling of neuronal activity with an underlying graph structure and follows from that to derive important theoretical results on a fixed environment. In Chapter 4, the model is adjusted to comport a random environment and asymptotic expressions are computed, showing interesting dependencies on the model parameters. Chapter 5 presents a brief discussion of the developments made and the possibilities that the future holds concerning this work.

Chapter 2

Concepts and Related Work

This chapter provides an overview of foundational concepts essential to understanding the key ideas investigated throughout the text. We begin by delving into neuroscience principles and exploring neuronal signalling and information transmission in the brain. Next, we introduce some important concepts of graph theory, focusing on random graphs and community structures. Finally, we provide the central notions of Markov chains. Section 2.4 discusses relevant prior works and how they relate to this dissertation's contributions.

2.1 Neuroscience Principles

In a nutshell, our nervous system is a network of interconnected cells called neurons, which communicate through electrical and chemical signals. These signals travel across synapses, connecting one neuron to the next. Every thought, action, and reaction we experience is due to the pathways of these signals.

Most neurons are, anatomically, subdivided into four main regions: dendrites, soma, axon, and axon terminals. Each of these regions plays a fundamental role in neuronal communication. Dendrites, which form an intricate branching structure known as the dendritic arbour, are primarily responsible for receiving input signals from other cells and transmitting them to the soma. In addition to containing the cell nucleus and other organelles, such as the endoplasmic reticulum, the soma is also the site where input signals are integrated. Those signals are then propagated along the axon, which can be cable-like and, in some cases, very long. Even though they travel considerable distances, the signals they carry are not significantly distorted or attenuated, a phenomenon attributed to two structures: the myelin sheath that insulates the axons and speeds up signal transmissions and the nodes of Ranvier, where the axon is exposed, and action potentials are regenerated. Axon terminals transmit signals to adjacent cells via chemical or electrical synapses, giving rise to the complex dynamics of neuronal communication. This phenomenon in which

signals travel in a specific direction, from dendrites to axon terminals, is called *dynamic polarization*, and it is a central principle in the connectionist approach to neuroscience studies (KANDEL *et al.*, 2000; COTMAN and MCGAUGH, 1980). Figure 2.1 depicts an illustrative diagram of a neuron's anatomy.

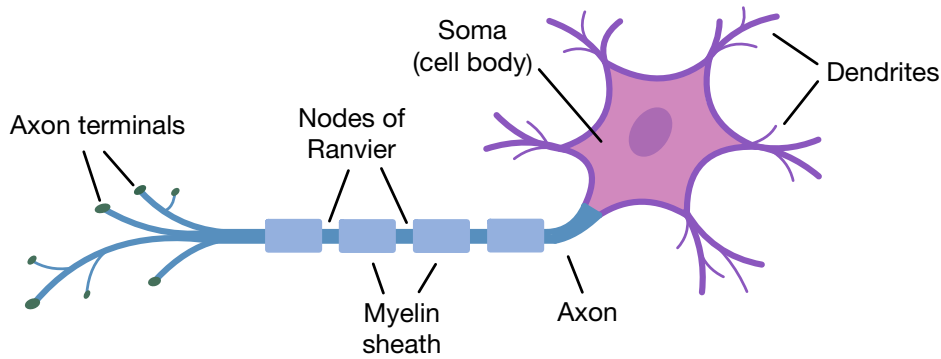


Figure 2.1: Diagram illustrating the main anatomical parts of a neuron, including the dendrites, soma, axon, and axon terminals.

The electrical signals neurons transmit are called *action potentials*. Neurons maintain a resting membrane potential, which is more negative than the external environment. When a neuron is sufficiently depolarized, its membrane potential reaches a critical voltage threshold, triggering an action potential. It is important to note that action potentials are *all-or-none events*. If the depolarization does not reach the voltage threshold, there is no action potential, but any depolarization above the threshold generates signals with the same magnitude (KANDEL *et al.*, 2000; COTMAN and MCGAUGH, 1980).

The sites where neurons transmit signals to other neurons are called synapses, which are classified into two types: electrical and chemical. In the case of an electrical synapse, gap-junction channels connect the cytoplasms of adjacent neurons, and ion currents directly transmit the action potential to the next cell in its pathway. Thanks to this direct connection, signalling has virtually no delay. In contrast, chemical synapses can be much more diverse. In this kind of synapse, which is the most common in our nervous system, action potentials in the presynaptic cell trigger the fusion of vesicles - containing neurotransmitters - with the cell membrane, and thus neurotransmitters are excreted to the synaptic cleft (a process known as exocytosis) and then bind to receptors located at the membrane of the postsynaptic cell. Because of this structure that involves neurotransmitters and receptors, chemical synapses can be *excitatory* or *inhibitory* and generate more significant changes in the postsynaptic cell. Neurons usually have thousands of input and output synapses, enabling intricate communication networks (KANDEL *et al.*, 2000; COTMAN and MCGAUGH, 1980).

Whether a signal is excitatory or inhibitory depends on the neurotransmitters released from the presynaptic terminals. Historically, all axonal branches of a neuron were believed to release the same neurotransmitter, a concept known as Dale's principle (DALE, 1935; ECCLES *et al.*, 1954). If this were true, all output signals from a single neuron would be of the same type, excitatory or inhibitory. However, this idea has been revised, and recent research has shown that mammalian neurons can produce and transmit both γ -aminobutyric acid (GABA) and glutamate (ROOT *et al.*, 2014), among other chemicals. GABA is the principal inhibitory neurotransmitter in mammals (BOONSTRA *et al.*, 2015; KOH *et al.*, 2023), while glutamate is the predominant excitatory neurotransmitter in the vertebrate nervous system (MELDRUM, 2000). This discovery challenges the paradigm that neurons are strictly excitatory or inhibitory. Instead, we should classify individual synapses based on the specific neurotransmitter being transferred.

As previously stated, inputs received through the dendrites are integrated at the cell's soma in a process known as neuronal integration. Multiple synaptic potentials are added together, and whether the neuron fires depends on whether the combined contributions are sufficient to depolarize the neuron's membrane to the threshold potential. Research suggests that most of these inputs are summed linearly (CASH and YUSTE, 1999).

On a more macro scale, the brain can be subdivided into regions associated with different functions. The patterns of interconnections between these regions play a key role in determining the function of neurons within the overall network of cells (BULLMORE and SPORNS, 2009). In this context, the brain network can be organized into clusters, which tend to have denser connections within themselves compared to the number of connections between different clusters (HILGETAG *et al.*, 2000).

These biological principles presented here provide a foundation for developing more realistically grounded mathematical models to simulate and predict neuronal behaviour in complex networks.

2.2 Random Graphs and Communities

Graphs are mathematical structures defined by an ordered pair of two sets $G = (V, E)$: one comprising the vertices, or nodes, (V) and the other comprising the edges (E), which represent the relationships or connections between vertices. Since their inception - often attributed to Euler's solution to the Bridges of Königsberg problem (EULER, 1736), depicted in Figure 2.2 - graphs have been widely used to model real-world problems. By providing an abstract representation, graphs simplify complex systems, making them easier to study and analyse from a mathematical

perspective.

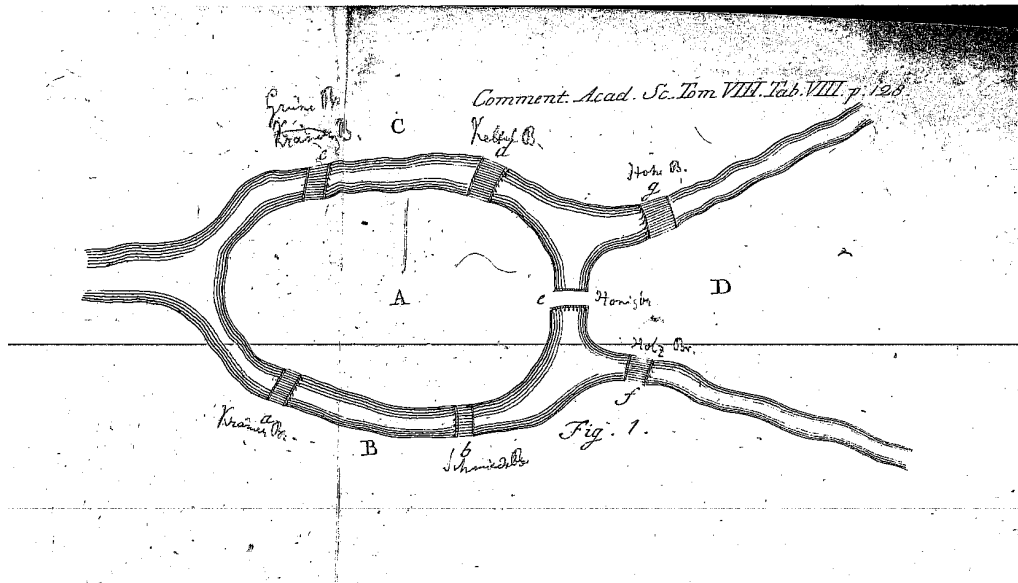


Figure 2.2: Euler's original drawing modelling the Königsberg bridges problem. Figure extracted from (EULER, 1736).

Graphs can emerge from random processes, representing samples from a probability distribution. Some classic random graph models are noteworthy. The original Erdős-Rényi model (ERDŐS and RÉNYI, 1959) constructs a graph by determining the number of nodes n and uniformly choosing m of its possible edges to exist. This model is now known as $G(n, m)$. A variation of it, known as $G(n, p)$, adds an edge between each pair of vertices following the output of a Bernoulli trial with a success rate p . The latter has been profoundly studied, with phase transitions for the emergence of specific topological properties being derived (FRIEZE and KAROŃSKI, 2015). Random models generate graphs with characteristics of real-world networks, such as the small-world property or the existence of hubs, presenting themselves as a valuable tool for understanding the emergence of these phenomena.

There are also graphs with community structures. In these cases, the set of vertices V is divided into communities (or blocks) with denser edges within each community and sparser edges between distinct communities, which reflects some real-world systems where interactions inside groups are more frequent.

Stochastic Block Model (SBM)

Combining these last two ideas, random constructions of graphs and community structures, the Stochastic Block Model (SBM) was created (HOLLAND *et al.*, 1983). In this model, vertices are divided into (usually) disjoint blocks, and each block has a specific probability distribution governing its edge existence to other blocks and within its set of vertices.

Mathematically speaking, let $\gamma : V \rightarrow \{1, 2, \dots, K\}$ be a function that assigns each vertex i to one of K blocks. The presence of an edge between two vertices, i and j , depends only on their block memberships and follows a Bernoulli distribution:

$$A_{ij} \sim \text{Bernoulli}(P_{\gamma(i), \gamma(j)}),$$

where A is the adjacency matrix of the graph, with $A_{ij} = 1$ indicating that there is an edge between i and j . P is a $K \times K$ matrix with entries $P_{k,l} \in [0, 1]$ representing the probability of having an edge from vertices in block k to vertices in block l . Figure 2.3 depicts a sample from the Stochastic Block Model with three blocks, illustrating how vertices within the same community tend to be more connected than those in different communities.

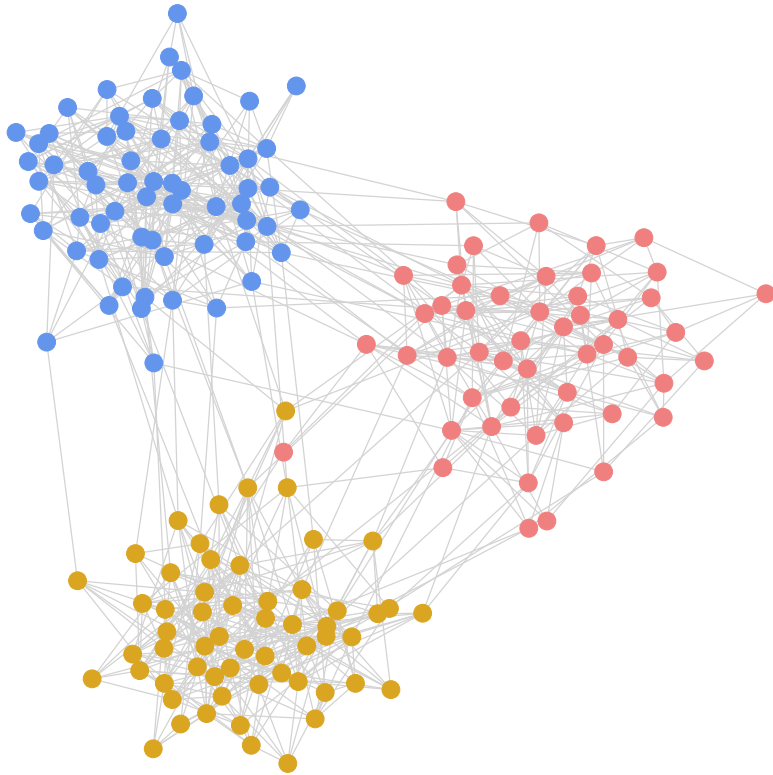


Figure 2.3: Sample from the Stochastic Block Model with three blocks. Vertices are coloured according to their block membership.

Results for large networks have shown that if the edge probability for intra-block edges and inter-block edges is sufficiently different, it is possible to recover the underlying community structure, that is, cluster vertices in correct blocks without knowing them *a priori* (AVRACHENKOV *et al.*, 2022). Nonetheless, this problem can be much more complicated if the communities overlap.

2.3 Markov Chains

Markov chains are stochastic processes with the memoryless property: the system's future state depends only on its current state and not on its previous history. Let X_0, X_1, X_2, \dots be a sequence of random variables taking values from a space state S . The process is Markovian if:

$$\mathbb{P}(X_{t+1} = x | X_0 = x_0, X_1 = x_1, \dots, X_t = x_t) = \mathbb{P}(X_{t+1} = x | X_t = x_t),$$

for all t .

Intuitively, we say that a Markov chain is aperiodic if there is no fixed cycle that forces a return to a state only after a certain number of steps. A state is aperiodic if the greatest common divisor of the number of steps it takes to return to that state is 1. A Markov chain is considered aperiodic if all its states are aperiodic. Another important concept is that of irreducibility. A Markov chain is irreducible if it is possible to reach any state from any other state, possibly through several steps (BROOKS *et al.*, 2011; HÄGGSTRÖM, 2002).

If a Markov chain converges to a specific distribution over its states, this distribution is called stationary. It is important to note that once the process reaches this distribution, it remains there indefinitely. A Markov chain that is both aperiodic and irreducible has a unique stationary distribution. Moreover, the long-term probability of being in any given state converges to its corresponding probability in the stationary distribution (BROOKS *et al.*, 2011; HÄGGSTRÖM, 2002).

2.4 Related Work

Many papers present studies addressing the challenge of inferring neuronal circuitry from spike train data (network recovery). A recent relevant work is KOBAYASHI *et al.* (2019), which seeks to discover the weighted adjacencies of the neuronal network and determine whether a neuron is excitatory or inhibitory. Their methodology applies a generalized linear model (GLM) to the cross-correlogram of spike train pairs, and significance thresholds are implemented to determine which inferred connections are statistically reliable. The estimation balances the antagonistic demands of reducing false positives and false negatives. However, the results are sensitive to the model's parameters, which must be tuned to achieve optimal performance. Additionally, many unconnected neuron pairs are wrongly assigned as connected due to indirect interactions through the network. These obstacles are exceeded in a subsequent work (ENDO *et al.*, 2021), where the authors propose a new method that presents high adaptability to different datasets and provides reasonable inference of

the neuronal circuitry. Although there is no need for parameter tuning, for being based on convolutional neural networks, this new attempt does not provide interpretability for its results, unlike the previous model with an interaction kernel to analyze the cross-correlograms.

REN *et al.* (2020) work on the same scenario, with a GLM describing correlograms between pairs of neurons, but incorporates information from latency between connected neurons’ spike trains to infer their distances better. They apply constraints to the model to rule out false positive estimations and better detect weak connections. However, to accomplish this goal, they rely on constraints based on expected structures that may be misleading if not correct.

LINDERMAN *et al.* (2016) proposes an efficient Bayesian framework to uncover latent structures in neuronal circuits, such as the spatial arrangement of neurons and their functional types. A GLM is used to model spike generation as a linear and autoregressive function of preceding spike counts of neighbouring neurons, and it is combined with graph-theoretical priors governing the relationship between latent features and neuronal connectivity patterns. Pólya-gamma augmentation enables collapsed Gibbs updates for the network and, therefore, efficient inference. For mapping activation levels to spike probabilities, logistic models were chosen to allow the application of the Pólya-gamma scheme. However, this choice could be a potential limitation since the framework cannot be directly applied to other widely used models in neuronal modelling.

Some papers focus only on clustering neurons in communities of the functional brain network. HUMPHRIES (2011) combines measures of spike-train comparison (Hamming distance and cosine similarity) with a modularity-based community detection framework. The similarity matrix is interpreted as a weighted network, and an eigenvector decomposition followed by K-means clustering is performed. The method self-determines the number of groups to maximize intra-group similarity. HERZOG *et al.* (2021) introduces a method based on Principal Component Analysis (PCA) and a density-based algorithm for clustering ensembles of neurons, that is, groups of neurons that exhibit synchronous activity. To validate the clusters returned by the algorithm, within-cluster correlations of spike trains are computed and compared with the whole population average correlation. Although these methods are validated on synthetic and real data sets, neither paper proposes a neuron-firing model nor provides any rigorous analysis of spike correlations.

Close to our setting, CHEVALLIER and OST (2024) introduce a neuronal firing model based on a subjacent random graph, where the network dynamics evolve as a stationary Markov chain. The transition probabilities governing neuron firing depend on the activity of adjacent neurons. The neurons are partitioned into two sets: \mathcal{P}_+ and \mathcal{P}_- , representing excitatory and inhibitory neurons, respectively. The

probability of neuron i firing, given the graph adjacency matrix θ and state x , is modelled as:

$$p_{\theta,i}(x) = \mu + (1 - \lambda) \left(\frac{1}{N} \sum_{j \in \mathcal{P}_+} \theta_{ij} x_j + \frac{1}{N} \sum_{j \in \mathcal{P}_-} \theta_{ij} (1 - x_j) \right).$$

This partition of the set of neurons into \mathcal{P}_+ and \mathcal{P}_- introduces a community structure, which the authors aim to detect solely from observed firing activity, without prior knowledge of other model parameters. Unlike most prior works, they provide a rigorous asymptotic analysis of the covariance matrix of spike trains. Under a separation condition on model parameters, they prove that exact community recovery is feasible with high probability.

It is important to note a key distinction between their work and ours: the underlying graph does not have a community structure in their model. Instead, the communities emerge from the roles of neurons in the network dynamics. In contrast, our model assumes a predefined community structure in the subjacent graph, where edges are assigned positive or negative weights corresponding to excitatory or inhibitory synapses. Despite these differences, the mathematical techniques used in our asymptotic analysis of the random environment in Chapter 4 closely follow the approach developed in their work (CHEVALLIER and OST, 2024).

Chapter 3

Neurons Firing Model with Communities (NFC) on a Fixed Environment

Section 3.1 presents a neuron-firing model with two communities where the interactions between neurons are fixed. Section 3.2 develops theoretical results to infer statistics from this model. Section 3.3 presents empirical analyses of actual networks and validates these theoretical results through stochastic simulations.

3.1 Modelling Neuronal Activity

Let $[N] = \{1, 2, \dots, N\}$ denote the set of neurons and let $\{C_1, C_2\}$ be a partition of $[N]$ representing two different communities of neurons. Let $\theta = (\theta_{ij})_{1 \leq i, j \leq N}$ be a $\{0, 1\}$ -matrix encoding the pairwise (directed) interaction between neurons: $\theta_{ij} = 0$ means that neuron i does not interact directly with neuron j , and $\theta_{ij} = 1$ otherwise. Note that the matrix θ does not need to be symmetric, which allows it to have, e.g., $\theta_{ij} = 0$ and $\theta_{ji} = 1$, and thus it can be interpreted as a directed graph. We shall assume that $\theta_{ii} = 0$ for all $i \in [N]$ (there are no self-loops). These modelling choices were made to better represent the dynamic polarization principle (2.1) and the fact that a presynaptic neuron sending signals to a postsynaptic neuron does not mean it receives signals back from it.

We write $i \sim j$ if and only if i and j belong to the same community, i.e., $i \sim j \iff (i, j) \in (C_1 \times C_1) \cup (C_2 \times C_2)$, and $i \not\sim j$ otherwise. Edges are classified as either *intra* or *inter*, depending on whether they connect neurons in the same community or across different communities, respectively. As we will see, the intensity of the interaction may differ depending on whether the corresponding edge is an intra- or inter-edge.

Additionally, each interaction in θ can be inhibitory or excitatory, and this is encoded in matrix $\eta = (\eta_{ij})_{1 \leq i, j \leq N}$ with $\{-1, 1\}$ -entries. Specifically, -1 indicates inhibitory adjacencies, while 1 represents excitatory adjacencies. Rather than modelling each neuron as inhibitory or excitatory, we model each adjacency as such to better reflect recent findings on neurotransmitters and synapses (see Section 2.1).

Let $G = (C_1 \cup C_2, \theta, \eta)$ be a directed weighted graph with N vertices summarizing all the network structures introduced above. Henceforth, we shall refer to G as the interaction graph.

As the firing of action potentials in neurons is an all-or-none event, the activity of neurons is here modelled via a system of N interacting $\{0, 1\}$ -valued random variables $\{X_{i,t}, i \in [N], t \in \{0\} \cup \mathbb{N}\}$, representing whether a neuron fires or not at a given time. Specifically, $X_{i,t} = 1$ means that neuron i fires at time t , and $X_{i,t} = 0$ means that neuron i does not fire at time t . These random variables are coupled through the interaction graph $G = (C_1 \cup C_2, \theta, \eta)$ as detailed below. Denoting by $X_t = (X_{1,t}, X_{2,t}, \dots, X_{N,t})$ the configuration of the system at time t , the process $\{X_t\}_{t \geq 0}$ evolves as a discrete-time Markov chain on the state space $\{0, 1\}^N$. The conditional distribution of X_t given $X_{t-1} = x$, where $x \in \{0, 1\}^N$, is that of N independent Bernoulli random variables with parameters $p_{G,i}(x)$, for $i \in [N]$. That is, for all $x, y \in \{0, 1\}^N$ and $t \geq 1$, we have

$$\mathbb{P}_G(X_t = y | X_{t-1} = x) = \prod_{i \in [N]} (p_{G,i}(x))^{y_i} (1 - p_{G,i}(x))^{1-y_i}, \quad (3.1)$$

where, given $x = (x_1, x_2, \dots, x_N) \in \{0, 1\}^N$,

$$p_{G,i}(x) = \mathbb{P}_G(X_{i,t} = 1 | X_{t-1} = x) = \lambda + \frac{\mu_{\sim}}{N} \sum_{j \sim i} \theta_{ji} \eta_{ji} x_j + \frac{\mu_{\not\sim}}{N} \sum_{j \not\sim i} \theta_{ji} \eta_{ji} x_j. \quad (3.2)$$

Equation (3.2) can be interpreted as the probability of neuron i firing at a given time based on the system's configuration at the preceding time step. The parameter $\lambda \in [0, 1]$ represents spontaneous activity, which is the same for all neurons. The first summation accounts for neurons within the same community as neuron i , while the second summation accounts for neurons in the other community. Both positive, μ_{\sim} and $\mu_{\not\sim}$ codify the intensity of interaction between neurons within the same community and between neurons in different communities, respectively. A neuron j interacting with neuron i ($\theta_{ji} = 1$) may either excite ($\eta_{ji} = 1$) or inhibit ($\eta_{ji} = -1$) neuron i 's activity, increasing or decreasing its firing probability by an amount of μ_{\sim}/N (if j and i are in the same community) or $\mu_{\not\sim}/N$ (if j and i are in different communities). Section 2.1 briefly discusses the motivation behind linearly summing the contributions of neurons.

In what follows, it will be convenient to express (3.2) in a matrix form. Thus, let $[N]$ be the set of neurons, $\{C_1, C_2\}$ be the partition of $[N]$ into two communities, and $G = (C_1 \cup C_2, \theta, \eta)$ be the interaction graph. We then introduce the corresponding interaction matrix $A = (A_{ij})_{1 \leq i, j \leq N}$, whose entries are defined as

$$A_{ij} := \frac{\mu_{\sim}}{N} \theta_{ij} \eta_{ij} \mathbb{1}_{\{i \sim j\}} + \frac{\mu_{\not\sim}}{N} \theta_{ij} \eta_{ij} \mathbb{1}_{\{i \not\sim j\}}. \quad (3.3)$$

To avoid clutter in the notation, we omit the dependence on G .

Then, for every $x \in \{0, 1\}^N$ and every $i \in [N]$, the firing probability $p_{G,i}(x)$ can be rewritten in a much simpler way as

$$p_{G,i}(x) = \lambda + (A^\top x)_i.$$

Note that for (3.1) to be well defined, we must have $p_{G,i}(x) \in [0, 1]$ for every $i \in [N]$ and every $x \in \{0, 1\}^N$. This need imposes some restrictions on the model parameters $\lambda, \mu_{\sim}, \mu_{\not\sim}$ and the interaction graph G . A sufficient condition is:

$$\mu_{\sim} \frac{\Delta_{\sim}}{N} + \mu_{\not\sim} \frac{\Delta_{\not\sim}}{N} < \lambda < 1 - \left(\mu_{\sim} \frac{\Delta_{\sim}}{N} + \mu_{\not\sim} \frac{\Delta_{\not\sim}}{N} \right) \iff \lambda \in (\|A^\top\|_\infty, 1 - \|A^\top\|_\infty), \quad (3.4)$$

where $\Delta_{\sim} = \max_i \sum_{j \sim i} \theta_{ji}$ is the maximal intra degree and $\Delta_{\not\sim} = \max_i \sum_{j \not\sim i} \theta_{ji}$ is the maximal inter degree. Observe that $\mu_{\sim} \Delta_{\sim} / N + \mu_{\not\sim} \Delta_{\not\sim} / N = \max_i \sum_{j \in [N]} |A_{ij}^\top| =: \|A^\top\|_\infty$. Thus, for (3.4) to be satisfied, it must necessarily be the case that $\|A^\top\|_\infty \leq 1/2$.

Throughout this text, we will work with a stationary version of this Markov chain, which in particular implies that $\mathbb{P}_G(X_t = x) = \mathbb{P}_G(X_0 = x)$ for all t and every $x \in \{0, 1\}^N$. Note that if (3.4) holds, then for every $i \in [N]$ and every $x \in \{0, 1\}^N$ we have $0 < p_{G,i} < 1$. The latter implies that we can reach every state from any other state. Hence, the Markov chain is irreducible and aperiodic, which, in turn, guarantees the existence of a unique stationary distribution.

3.2 Theoretical Results

We begin by defining some important quantities.

Definition 3.1. We define *firing mean* as the column vector m with entries given by $m_i := \mathbb{P}_G(X_{i,t} = 1)$, for all $i \in [N]$. *Firing variance* is the column vector v with entries $v_i = m_i(1 - m_i)$, for all $i \in [N]$. *Synchronous firing covariance* is the matrix $\Sigma^{(0)} = \left(\Sigma_{ij}^{(0)} \right)_{1 \leq i, j \leq N}$ with entries defined as

$$\Sigma_{ij}^{(0)} = \text{Cov}_G(X_{i,0}, X_{j,0}).$$

One-lagged firing covariance is the matrix $\Sigma^{(1)} = \left(\Sigma_{ij}^{(1)} \right)_{1 \leq i, j \leq N}$ with entries defined as

$$\Sigma_{ij}^{(1)} = \text{Cov}_G(X_{i,1}, X_{j,0}).$$

Theorem 3.1 (Firing mean). *Let $[N]$ be the set of neurons, $\{C_1, C_2\}$ the two communities, $G = (C_1 \cup C_2, \theta, \eta)$ the interaction graph, and $\lambda \in [0, 1]$ the spontaneous activity. Assume that the corresponding interaction matrix A and λ satisfy (3.4). Then, the firing mean m is given by*

$$m = (I_N - A^\top)^{-1} \lambda \mathbf{1}_N \stackrel{(*)}{=} \lambda \sum_{z=0}^{\infty} (A^\top)^z \mathbf{1}_N, \quad (3.5)$$

where $\mathbf{1}_N$ denotes a column vector of length N with all entries equal to 1 and I_N is the N -dimensional identity matrix. In (*), we use the geometric series of matrices.

Proof. For each $i \in [N]$, we have

$$m_i = \mathbb{P}_G(X_{i,t} = 1) = \mathbb{E}_G[\mathbb{P}_G(X_{i,t}|X_{t-1})].$$

Using (3.2) in the latter expression, we obtain that

$$\begin{aligned} m_i &= \mathbb{E}_G \left[\lambda + \frac{\mu_{\sim}}{N} \sum_{j \sim i} \theta_{ji} \eta_{ji} X_{j,t-1} + \frac{\mu_{\not\sim}}{N} \sum_{j \not\sim i} \theta_{ji} \eta_{ji} X_{j,t-1} \right] \\ &= \lambda + \frac{\mu_{\sim}}{N} \sum_{j \sim i} \theta_{ji} \eta_{ji} \mathbb{E}_G[X_{j,t-1}] + \frac{\mu_{\not\sim}}{N} \sum_{j \not\sim i} \theta_{ji} \eta_{ji} \mathbb{E}_G[X_{j,t-1}] \\ &\stackrel{(*)}{=} \lambda + \frac{\mu_{\sim}}{N} \sum_{j \sim i} \theta_{ji} \eta_{ji} m_j + \frac{\mu_{\not\sim}}{N} \sum_{j \not\sim i} \theta_{ji} \eta_{ji} m_j, \end{aligned} \quad (3.6)$$

where in (*) we used the assumption that the Markov chain $\{X_t\}_{t \geq 0}$ is stationary, which implies that $m_i = \mathbb{E}_G[X_{i,t}]$, for all t . Since (3.6) holds for all $i \in [N]$, setting $m = (m_1, m_2, \dots, m_N)^\top$, we can rewrite the system of equations in a matrix form as follows:

$$m = \lambda \mathbf{1}_N + A^\top m \iff (I_N - A^\top) m = \lambda \mathbf{1}_N.$$

Under the assumption that A and λ satisfy (3.4), the matrix $(I_N - A^\top)$ is invertible, and the claim follows. \square

Example 3.2.1. Consider $\lambda = 0.25$ and the following interaction matrix:

$$A = \frac{1}{4} \begin{bmatrix} 0 & 0 & 0.2 & 0.2 \\ 0 & 0 & 0.2 & 0.2 \\ 0 & 0 & 0 & 0 \\ 0 & 0 & 0 & 0 \end{bmatrix}.$$

Figure 3.1 depicts the corresponding adjacency matrix.

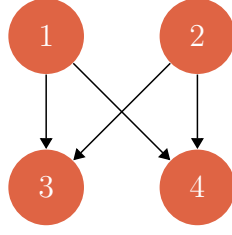


Figure 3.1: Example graph

We can compute the firing mean for each neuron through Equation (3.5), which yields

$$m = \begin{bmatrix} 0.25 & 0.25 & 0.275 & 0.275 \end{bmatrix}^\top.$$

Notice that neurons with no incoming edges (1 and 2) have a firing mean equal to the spontaneous activity, as expected. In contrast, neurons 3 and 4 exhibit an increased firing mean due to the excitatory inputs from neurons 1 and 2.

Before stating our next result, we need to define some operations. Given an N -dimensional vector w , we define $\text{diag}(w)$ as the $N \times N$ diagonal matrix with diagonal entries $\text{diag}(w)_{ii} = w_i$, $i \in [N]$. Additionally, given an $N \times N$ matrix M , we define $d(M)$ as the diagonal matrix obtained by setting all off-diagonal elements of M to zero while leaving the diagonal elements unchanged.

Example 3.2.2. Let $w = \begin{bmatrix} 1 & 2 & 3 \end{bmatrix}^\top$. Then,

$$\text{diag}(w) = \begin{bmatrix} 1 & 0 & 0 \\ 0 & 2 & 0 \\ 0 & 0 & 3 \end{bmatrix}.$$

Now, let $M = \begin{bmatrix} 1 & 2 & 3 \\ 4 & 5 & 6 \\ 7 & 8 & 9 \end{bmatrix}$. Then,

$$d(M) = \begin{bmatrix} 1 & 0 & 0 \\ 0 & 5 & 0 \\ 0 & 0 & 9 \end{bmatrix}.$$

Theorem 3.2 (Synchronous firing covariance). *Let $[N]$ be the set of neurons, $\{C_1, C_2\}$ the two communities, and $G = (C_1 \cup C_2, \theta, \eta)$ the interaction graph. Assume that the corresponding interaction matrix A satisfies (3.4). Then, the synchronous firing covariance matrix is the unique solution of the following matrix*

equation:

$$\Sigma^{(0)} = A^\top \Sigma^{(0)} A - d(A^\top \Sigma^{(0)} A) + \text{diag}(v), \quad (3.7)$$

where v is the firing variance.

Proof. Let us begin by observing that, for all $i \in [N]$, $\Sigma_{ii}^{(0)} = \text{Var}[X_{i,0}] = v_i$, thus (3.7) is satisfied for the diagonal elements. Since the Markov chain $\{X_t\}_{t \geq 0}$ is stationary, we have

$$\mathbb{E}[X_{i,t} X_{j,t}] = \mathbb{E}[X_{i,0} X_{j,0}],$$

for all t and for $i, j \in [N]$.

Consequently,

$$\begin{aligned} \Sigma_{ij}^{(0)} &= \text{Cov}_G(X_{i,1}, X_{j,1}) = \mathbb{E}_G[X_{i,1} X_{j,1}] - \mathbb{E}_G[X_{i,1}] \mathbb{E}_G[X_{j,1}] \\ &= \mathbb{E}_G[\mathbb{E}_G[X_{i,1} X_{j,1} | X_0]] - m_i m_j \\ &\stackrel{(*)}{=} \mathbb{E}_G[\mathbb{E}_G[X_{i,1} | X_0] \mathbb{E}_G[X_{j,1} | X_0]] - m_i m_j \\ &= \mathbb{E}_G\left[(\lambda + (A^\top X_0)_i) (\lambda + (A^\top X_0)_j)\right] - \\ &\quad - \mathbb{E}_G[(\lambda + (A^\top X_0)_i)] \mathbb{E}_G[(\lambda + (A^\top X_0)_j)] \end{aligned}$$

where in (*), we used the conditional independence of the model. Using further the linearity of the expectation, we obtain that

$$\begin{aligned} \Sigma_{ij}^{(0)} &= \mathbb{E}_G\left[(A^\top X_0)_i (A^\top X_0)_j\right] - (A^\top \mathbb{E}_G[X_0])_i (A^\top \mathbb{E}_G[X_0])_j \\ &= \sum_{k \in [N]} \sum_{l \in [N]} A_{ik}^\top \mathbb{E}_G[X_{k,0} X_{l,0}] A_{jl}^\top - \sum_{k \in [N]} A_{ik}^\top \mathbb{E}_G[X_{k,0}] \sum_{l \in [N]} A_{jl}^\top \mathbb{E}_G[X_{l,0}] \\ &= \sum_{k \in [N]} \sum_{l \in [N]} A_{ik}^\top (\mathbb{E}_G[X_{k,0} X_{l,0}] - \mathbb{E}_G[X_{k,0}] \mathbb{E}_G[X_{l,0}]) A_{jl}^\top \\ &= \sum_{k \in [N]} \sum_{l \in [N]} A_{ik}^\top \Sigma_{kl}^{(0)} A_{jl}^\top \\ &= (A^\top \Sigma^{(0)} A)_{ij}, \end{aligned}$$

and thus, (3.7) is also satisfied for the off-diagonal entries. \square

Note, however, that $\Sigma^{(0)}$ appears on both sides of the equation, which does not provide a direct solution for the synchronous firing covariance. Corollary 3.2.1 provides a way to analytically address this problem. But before stating it, we shall introduce some notations. Given an $N \times N$ matrix M , $\text{vec}(M)$ denotes its vectorization, i.e., the N^2 -dimensional column vector obtained by stacking the columns of M one after the other. Specifically, for $k \in [N^2]$, we have $\text{vec}(M)_k = M_{ij}$, where $i, j \in [N]$ are uniquely determined by $k = N(j-1) + i$. Moreover, given two $N \times N$ matrices B and C , their Kronecker product $B \otimes C$ is defined as the $N^2 \times N^2$ matrix

whose entries are given by $(B \otimes C)_{su} = B_{ik}C_{jl}$, where $i, j, k, l \in [N]$ are uniquely determined by $s = N(i-1) + j$ and $u = N(k-1) + l$. The Kronecker product and the vectorization operation are related by the following property: given three matrices B, C, M , it holds that $\text{vec}(BMC) = (C^\top \otimes B) \text{vec}(M)$.

Example 3.2.3. Let $M = \begin{bmatrix} 1 & 2 & 3 \\ 4 & 5 & 6 \\ 7 & 8 & 9 \end{bmatrix}$. Then,

$$\text{vec}(M) = \begin{bmatrix} 1 & 4 & 7 & 2 & 5 & 8 & 3 & 6 & 9 \end{bmatrix}^\top.$$

Now, let $B = \begin{bmatrix} 1 & 2 \\ 3 & 4 \end{bmatrix}$ and $C = \begin{bmatrix} 5 & 6 \\ 7 & 8 \end{bmatrix}$. Then,

$$B \otimes C = \begin{bmatrix} 1 \cdot C & 2 \cdot C \\ 3 \cdot C & 4 \cdot C \end{bmatrix} = \begin{bmatrix} 5 & 6 & 10 & 12 \\ 7 & 8 & 14 & 16 \\ 15 & 18 & 20 & 24 \\ 21 & 24 & 28 & 32 \end{bmatrix}.$$

Corollary 3.2.1. *In a vectorized form, the unique solution of (3.7) is given by*

$$\text{vec}(\Sigma^{(0)}) = (I_{N^2} - L)^{-1} \text{vec}(\text{diag}(v)) = \sum_{z=0}^{\infty} L^z \text{vec}(\text{diag}(v)), \quad (3.8)$$

where I_{N^2} is the N^2 -dimensional identity matrix and L is an $N^2 \times N^2$ matrix whose entries are defined as

$$L_{su} = \begin{cases} 0 & \text{if } s = N(i-1) + i, \text{ for } i \in [N], \\ (A^\top \otimes A^\top)_{su} & \text{otherwise.} \end{cases}$$

Proof. The vectorization operator $\text{vec}(\cdot)$ is linear and invertible. Therefore, the unique solution of (3.7) in a vectorized form is the solution of the following equation

$$\text{vec}(\Sigma^{(0)}) = \text{vec}(A^\top \Sigma^{(0)} A) - \text{vec}(d(A^\top \Sigma^{(0)} A)) + \text{vec}(\text{diag}(v)). \quad (3.9)$$

Note that, since $d(A^\top \Sigma^{(0)} A)$ is a diagonal matrix, many entries of the vector $\text{vec}(d(A^\top \Sigma^{(0)} A))$ are equal to zero. Specifically, the only non-zero entries are those with index $s = N(i-1) + i$, with $i \in [N]$ and they are equal to $\text{vec}(d(A^\top \Sigma^{(0)} A))_s =$

$(A^\top \Sigma^{(0)} A)_{ii}$. The latter can be rewritten as

$$(A^\top \Sigma^{(0)} A)_{ii} = \sum_{k \in [N]} \sum_{l \in [N]} A_{ik}^\top \Sigma_{kl}^{(0)} A_{li} = \sum_{k \in [N]} \sum_{l \in [N]} A_{ik}^\top A_{il}^\top \Sigma_{kl}^{(0)} = \sum_{u=1}^{N^2} F_{su} \text{vec}(\Sigma^{(0)})_u,$$

where $F_{su} = A_{ik}^\top A_{il}^\top$ with $k, l \in [N]$ uniquely determined by $u = N(k-1) + l$. Thus, by defining F as an $N^2 \times N^2$ matrix with entries

$$F_{su} = \begin{cases} (A^\top \otimes A^\top)_{su} & \text{if } s = N(i-1) + i, \text{ for } i \in [N], \\ 0 & \text{otherwise,} \end{cases}$$

we obtain that $\text{vec}(d(A^\top \Sigma^{(0)} A)) = F \text{vec}(\Sigma^{(0)})$. Additionally, using the fact that $\text{vec}(A^\top \Sigma^{(0)} A) = (A^\top \otimes A^\top) \text{vec}(\Sigma^{(0)})$, (3.9) can be rewritten as

$$\text{vec}(\Sigma^{(0)}) = (A^\top \otimes A^\top) \text{vec}(\Sigma^{(0)}) - F \text{vec}(\Sigma^{(0)}) + \text{vec}(\text{diag}(v)).$$

By setting $L = A^\top \otimes A^\top - F$, we obtain that $(I_{N^2} - L) \text{vec}(\Sigma^{(0)}) = \text{vec}(\text{diag}(v))$. The proof then follows once we note that $(I_{N^2} - L)$ is invertible, which is verified by observing that

$$\|L\|_\infty = \max_s \sum_{u=1}^{N^2} |L_{su}| = \max_{i \neq j} \sum_{k \in [N]} \sum_{l \in [N]} |A_{ik}^\top| |A_{jl}^\top| \leq \|A^\top\|_\infty^2.$$

The above bound and the assumption that A satisfies (3.4) implies that $\|L\|_\infty < 1$, which in turn assures that $(I_{N^2} - L)$ is invertible. \square

Proposition 3.3 (One-lagged firing covariance). *The one-lagged and the synchronous firing covariances are related by*

$$\Sigma^{(1)} = A^\top \Sigma^{(0)}.$$

Proof. For $i, j \in [N]$, we have

$$\begin{aligned} \Sigma_{ij}^{(1)} &= \text{Cov}_G(X_{i,1}, X_{j,0}) = \mathbb{E}_G[X_{i,1} X_{j,0}] - m_i m_j \\ &= \mathbb{E}_G[\mathbb{E}_G[X_{i,1} X_{j,0} | X_0]] - m_i m_j \\ &= \mathbb{E}_G[X_{j,0} \mathbb{E}_G[X_{i,1} | X_0]] - m_i m_j \\ &= \mathbb{E}_G[X_{j,0} (\lambda + (A^\top X_0)_i)] - m_i m_j \\ &= m_j \lambda + \mathbb{E}_G[X_{j,0} (A^\top X_0)_i] - m_i m_j. \end{aligned}$$

Using the definition of matrix A (Equation (3.3)), the term $\mathbb{E}_G[X_{j,0} (A^\top X_0)_i]$

can be rewritten as

$$\begin{aligned}
\mathbb{E}_G [X_{j,0} (A^\top X_0)_i] &= \mathbb{E}_G \left[X_{j,0} \left(\frac{\mu_{\sim}}{N} \sum_{k \sim i} \theta_{ki} \eta_{ki} X_{k,0} + \frac{\mu_{\not\sim}}{N} \sum_{k \not\sim i} \theta_{ki} \eta_{ki} X_{k,0} \right) \right] \\
&= \frac{\mu_{\sim}}{N} \sum_{k \sim i} \theta_{ki} \eta_{ki} \mathbb{E}_G [X_{k,0} X_{j,0}] + \frac{\mu_{\not\sim}}{N} \sum_{k \not\sim i} \theta_{ki} \eta_{ki} \mathbb{E}_G [X_{k,0} X_{j,0}] \\
&= (A^\top \Sigma^{(0)})_{ij} + m_j \sum_{k \in [N]} A_{ki}^\top m_k.
\end{aligned}$$

Overall, we then obtain that $\Sigma_{ij}^{(1)} = (A^\top \Sigma^0)_{ij} + m_j \left(\lambda + \sum_{k \in [N]} A_{ki}^\top m_k \right) - m_i m_j$. Using that

$$m_i = \mathbb{E}_G [X_{i,1}] = \mathbb{E}_G [\mathbb{E}_G [X_{i,1} | X_0]] = \mathbb{E}_G [\lambda + (A^\top X_0)_i] = \lambda + \sum_{k \in [N]} A_{ki}^\top m_k,$$

the proof is complete. \square

A direct consequence of Proposition 3.3 and Corollary 3.2.1 is that the one-lagged covariance can be computed by

$$\begin{aligned}
\text{vec} (\Sigma^{(1)}) &= \text{vec} (A^\top \Sigma^{(0)}) \\
&= (I_N \otimes A^\top) \text{vec} (\Sigma^{(0)}) \\
&= (I_N \otimes A^\top) (I_{N^2} - L)^{-1} \text{vec} (\text{diag} (v)).
\end{aligned}$$

Example 3.2.4. Returning to the setting of Example 3.2.1 where $\lambda = 0.25$ and

$$A = \frac{1}{4} \begin{bmatrix} 0 & 0 & 0.2 & 0.2 \\ 0 & 0 & 0.2 & 0.2 \\ 0 & 0 & 0 & 0 \\ 0 & 0 & 0 & 0 \end{bmatrix},$$

we already computed that

$$m = \left[0.25 \quad 0.25 \quad 0.275 \quad 0.275 \right]^\top.$$

Thus, by the definition of firing variance,

$$v = \left[0.1875 \quad 0.1875 \quad 0.199375 \quad 0.199375 \right]^\top.$$

Using these values, we can compute the synchronous firing covariance as

$$\Sigma^{(0)} = \begin{bmatrix} 0.1875 & 0 & 0 & 0 \\ 0 & 0.1875 & 0 & 0 \\ 0 & 0 & 0.199375 & 0.0009375 \\ 0 & 0 & 0.0009375 & 0.199375 \end{bmatrix},$$

as well as the one-lagged firing covariance

$$\Sigma^{(1)} = \begin{bmatrix} 0 & 0 & 0.01001563 & 0.01001563 \\ 0 & 0 & 0.01001563 & 0.01001563 \\ 0 & 0 & 0 & 0 \\ 0 & 0 & 0 & 0 \end{bmatrix}.$$

Note how, in the last example (3.2.4), the off-diagonal values of the one-lagged firing covariance are significantly larger than those in the synchronous firing covariance. In addition, these values are more closely tied to the graph's edges; that is, the covariance is non-zero for adjacent neurons. In contrast, in the synchronous case, off the main diagonal, the neurons with non-zero covariance values are those that share common neighbours. These phenomena suggest that, while the former reflects direct connections in the graph, the latter captures more indirect interactions through mutual connections, as expected, given the time delay and model premises. Thus, both covariances provide complementary information about the structure of the underlying network.

3.3 Empirical and Numerical Analyses

In the previous section, we derived some theoretical results from the neuronal activity model presented in Section 3.1. Now, we proceed with empirical analyses and numerical validation. This should provide an intuitive understanding of the model parameters and their influence on certain computed statistics.

We sample graphs from the SBM model with parameters p and q (the intra- and inter-community edge probabilities) to generate the graphs and conduct this empirical analysis on actual networks. Additionally, we sample the η matrix as follows:

$$\eta_{ij} = \begin{cases} 1 & \text{with probability } \beta, \\ -1 & \text{with probability } 1 - \beta. \end{cases} \quad (3.10)$$

Figure 3.2 depicts the cumulative distribution function (CDF) for the firing mean of neurons in networks sampled from the SBM model across different scenarios (with varying β , μ_{\sim} , $\mu_{\not\sim}$, and q). For all experiments, we assume the spontaneous activity

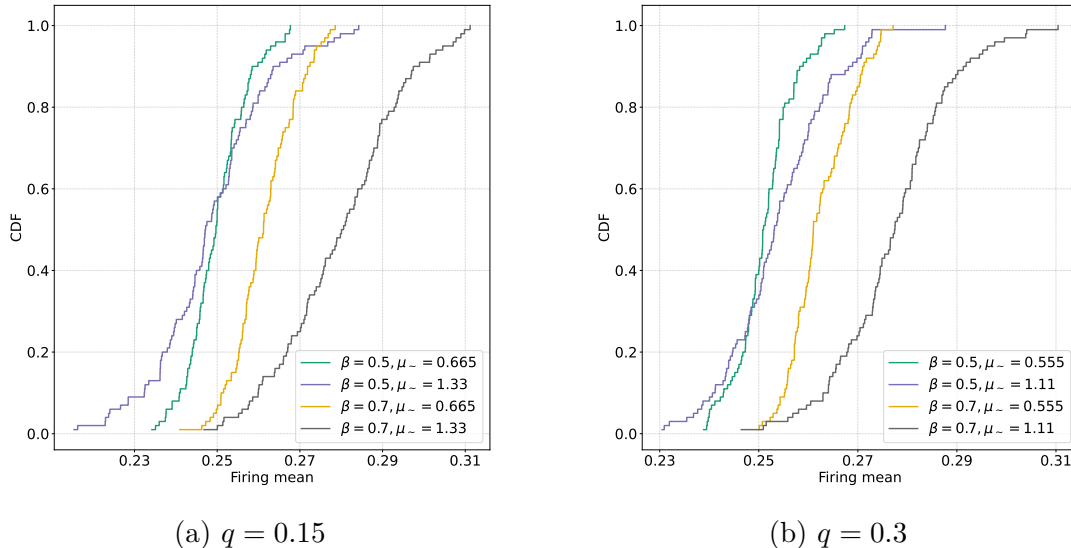


Figure 3.2: Firing mean CDF for networks sampled from the SBM model with intra-community edge probability $p = 0.3$ and $N = 100$ neurons. The other parameters for the neuronal activity model are $\lambda = 0.25$ and $\mu_{\neq} = \mu_{\sim}/2$.

rate to be constant at $\lambda = 0.25$ and set $\mu_{\neq} = \mu_{\sim}/2$ for all experiments. When μ_{\sim} is smaller and $\beta = 0.5$, the firing mean values are more concentrated around the spontaneous activity rate. However, for larger values of μ_{\sim} , the distribution spans a broader range of values. The parameter β (the probability of an excitatory edge) shifts the CDF curves horizontally. Specifically, when $\beta > 0.5$, the centre of the distribution shifts to higher values of firing mean, as expected, since a higher proportion of excitatory edges results in more frequent firing. Interestingly, there is little dependence on the variation of the proportion p/q .

Figures 3.3 and 3.4 present experiments conducted similarly to the one discussed in Figure 3.2, but with a focus on covariance values. It is important to note that covariance values can be negative or positive and typically fall within a relatively narrow range. The larger the values of μ_{\sim} and μ_{\neq} , the stronger the covariance between neurons' firing, as the firing of one neuron has a more substantial effect on its neighbours. Figure 3.3 depicts the CDF for synchronous firing covariance, while Figure 3.4 displays the CDF for one-lagged firing covariance. The former predominantly exhibits smaller values (in magnitude). In contrast, although the latter contains many zero values, it also includes larger values that deviate further from zero. This pattern aligns with expectations. As suggested in Example 3.2.4 and discussed in Section 3.2, synchronous firing covariance captures more indirect interactions, which are more common than direct interactions, leading to a higher frequency of non-zero values. In contrast, one-lagged firing covariance highlights direct connections, which tend to be stronger.

While covariance values are small, their structure is far from random. Figure

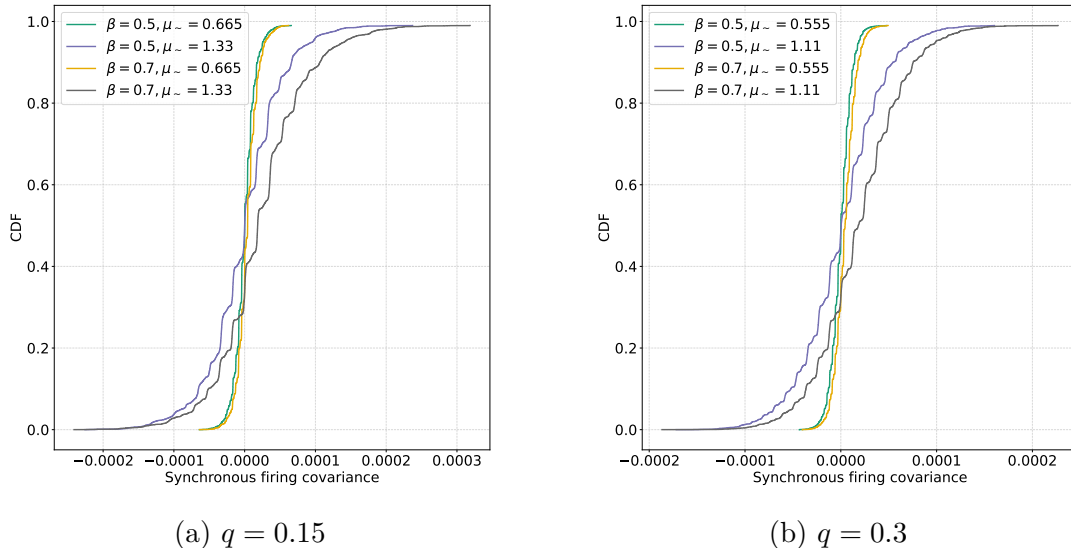


Figure 3.3: Synchronous firing covariance CDF for networks sampled from the SBM model with intra-community edge probability $p = 0.3$ and $N = 100$ neurons. The other parameters for the neuronal activity model are $\lambda = 0.25$ and $\mu_{\gamma} = \mu_{\sim}/2$.

3.5 depicts the pairwise covariance for synchronous and one-lagged neurons' firing in networks with 100 nodes. Note that high covariance values (in magnitude) occur more frequently between pairs of neurons within the same community. This observation is much stronger for one-lagged firing covariance, where high absolute covariance values occur more frequently - mainly within a community - and the separation between intra- and inter-community covariances becomes clearer (as shown by the scale of the values in the graphs).

To validate these theoretical results, we compare them with statistics obtained from a stochastic simulator that generates spike trains based on the neuronal activity model presented in Section 3.1. This simulator was first introduced in (COELHO *et al.*, 2025) and described in detail in (COELHO, 2025). It is also available online at <https://github.com/Thiagohnc/neuroscience>.

In each experiment, we generate samples from an SBM model with two communities and parameters p and q (intra- and inter-community edge probabilities, respectively). We sample the corresponding excitatory/inhibitory matrix η as given in Equation (3.10). Subsequently, we use the simulator to generate a time series of binary spike trains for each neuron over T time steps. From these time series, we compute the average firing rate for each neuron and the pairwise correlations between the neurons' spike trains.

We then compare each graph's theoretical firing mean m with the average firing rate obtained from the simulated spike trains.

Given a graph G , let m_i denote the theoretical firing mean of neuron i and $\hat{m}_i(T)$ denote the sample average firing rate of neuron i computed from a spike

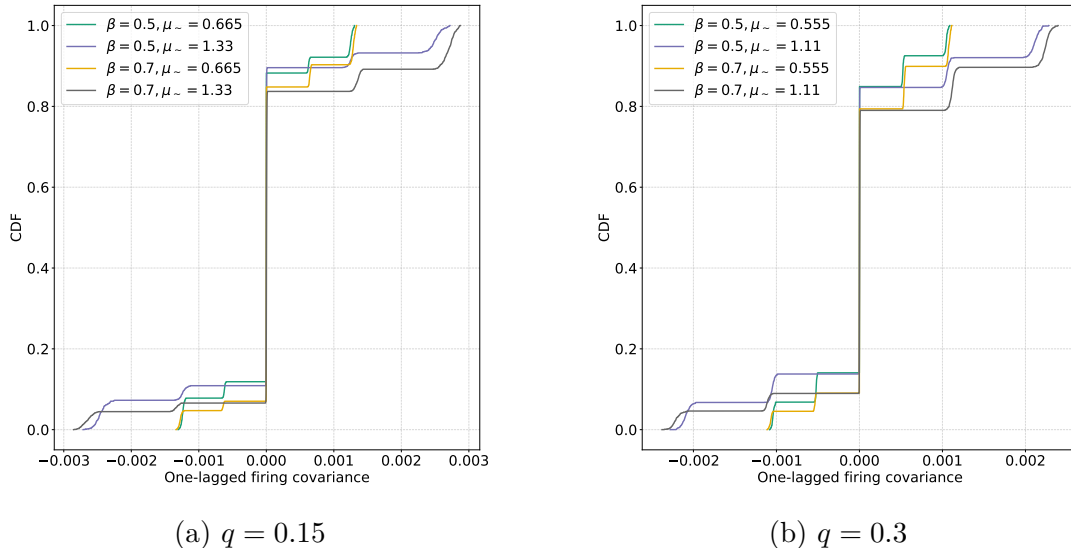


Figure 3.4: One-lagged firing covariance CDF for networks sampled from the SBM model with intra-community edge probability $p = 0.3$ and $N = 100$ neurons. The other parameters for the neuronal activity model are $\lambda = 0.25$ and $\mu_{\gamma} = \mu_{\sim}/2$.

train of length T . We define the mean absolute error for the firing rate as $E_m(T) = \frac{1}{N} \sum_i |m_i - \hat{m}_i(T)|$. Assuming that G is drawn from the SBM model (with edges being excitatory or inhibitory) and that we have r independent samples of G , the expected mean absolute error can be estimated by averaging the errors over these samples.

Figure 3.6 shows the expected mean absolute error as a function of T for different scenarios. Note that the error decays proportionally to \sqrt{T} (i.e., the curves have a slope near 0.5). The absolute error is not significantly affected by the model parameters: N , community sizes, μ_{\sim} , μ_{γ} , p and q .

In the next experiment, we also compute the theoretical correlations. The synchronous firing correlation is given by

$$C_{ij}^{(0)} = \frac{\Sigma_{ij}^{(0)}}{\sqrt{v_i} \sqrt{v_j}}, \quad (3.11)$$

where $\Sigma^{(0)}$ is the theoretical synchronous firing covariance and v_i is the theoretical firing variance of neuron i . We similarly define the one-lagged firing correlation as

$$C_{ij}^{(1)} = \frac{\Sigma_{ij}^{(1)}}{\sqrt{v_i} \sqrt{v_j}}.$$

Given a graph G , let $\hat{C}^{(0)}(T)$ and $\hat{C}^{(1)}(T)$ denote the empirical synchronous firing correlation and one-lagged firing correlation, respectively, computed from spike trains of length T for all pairs of neurons. The mean absolute error of the correlations

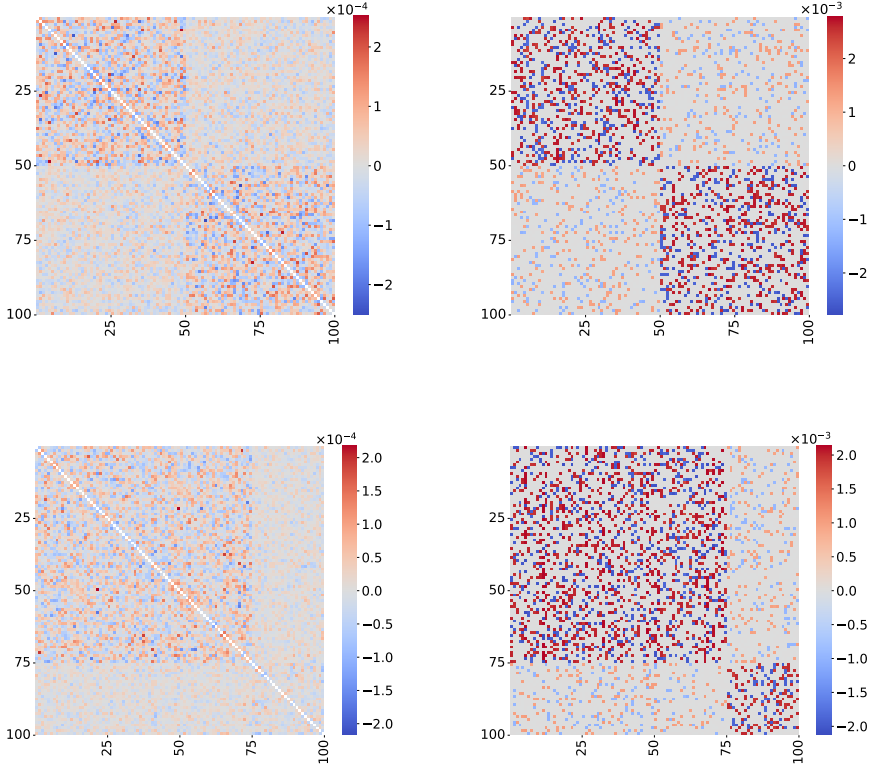


Figure 3.5: Covariance heatmaps for networks with $N = 100$ neurons. In the first row, both communities contain 50 neurons, while in the second row, the communities consist of 75 and 25 neurons. The left column shows the synchronous firing covariance and the right column shows the one-lagged firing covariance. The other model parameters are $\lambda = 0.25$, $p = 0.3$, $q = 0.15$, $\beta = 0.6$, $\mu_{\sim} = 1.33$ (first row) and $\mu_{\sim} = 1.02$ (second row), and $\mu_{\neq} = \mu_{\sim}/2$.

is computed by comparing these empirical values with the theoretical correlations $C^{(0)}$ and $C^{(1)}$. When G is drawn from the SBM model and r independent samples are available, averaging over the samples estimates the expected mean absolute error.

Figure 3.7 shows the expected mean absolute error of the correlations as a function of T . In both the synchronous and one-lagged cases, the convergence of the estimated correlations to the theoretical values is robust with respect to changes in the model parameters.

For the covariance and correlation experiments in the synchronous case, we omit the values for $i = j$ because they are so much larger than the others that they would overwhelm the analysis and mask meaningful information.

In conclusion, the spike train length is the primary factor in the numerical validations, as it can significantly influence the empirical evaluation - particularly given the minimal magnitude of the correlation values.

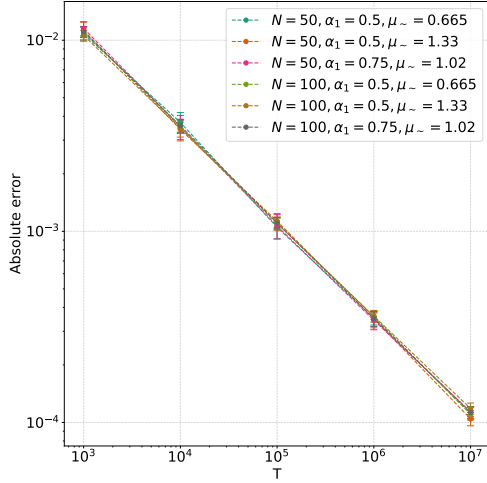
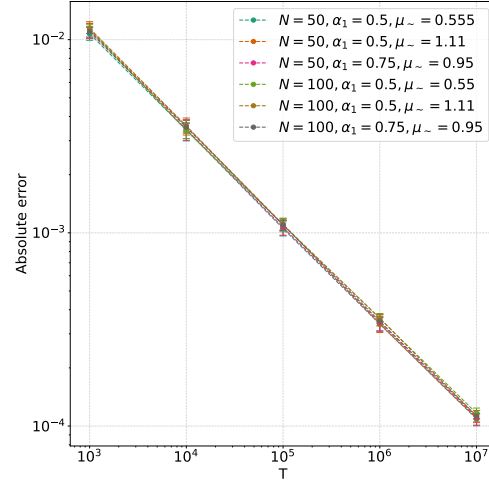
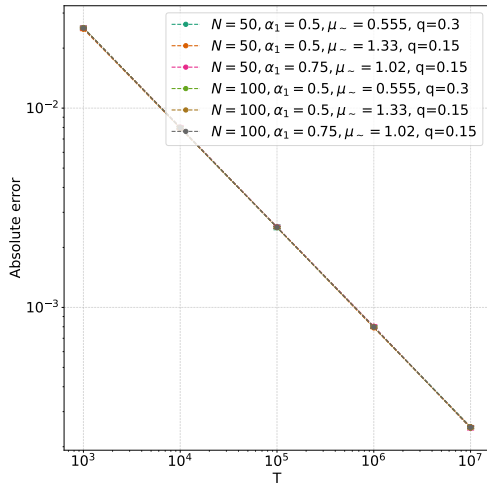
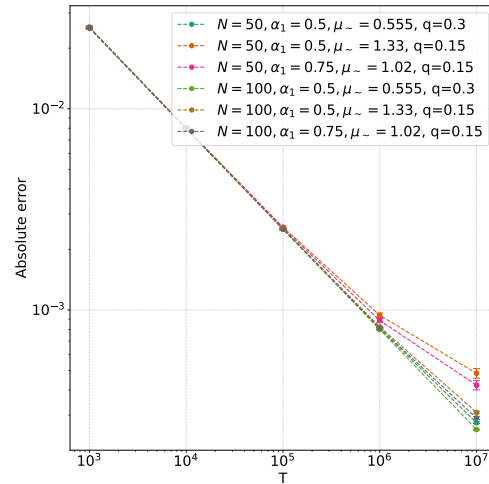
(a) $q = 0.15$ (b) $q = 0.3$

Figure 3.6: Expected mean absolute error for the firing rate of neurons in networks sampled from the SBM model with intra-community edge probability $p = 0.3$. Additionally, $\beta = 0.6$. The parameters for the neuronal activity model are $\lambda = 0.25$, and $\mu_{\gamma} = \mu_{\sim}/2$. Here, α_1 denotes the proportion of neurons in community 1, i.e., $\alpha_1 = |C_1|/N$. The plots are shown in a log-log scale. For each T , $r = 10$ networks were generated, and the average error and one standard deviation are shown.



(a) Synchronous firing correlation



(b) One-lagged firing correlation

Figure 3.7: Expected mean absolute error for the correlations in networks sampled from the SBM model with intra-community edge probability $p = 0.3$. Additionally, $\beta = 0.6$. The parameters for the neuronal activity model are $\lambda = 0.25$, and $\mu_{\gamma} = \mu_{\sim}/2$. Here, α_1 denotes the proportion of neurons in community 1, i.e., $\alpha_1 = |C_1|/N$. The plots are shown in a log-log scale. For each T , $r = 10$ networks were generated, and the average error and one standard deviation are shown.

Chapter 4

Neurons Firing Model with Communities (NFC) on a Random Environment

This chapter considers the NFC in a random environment when the underlying interaction graph is random. Specifically, given a set of neurons $[N]$ and two communities $\{C_1, C_2\}$, we assume that the matrix encoding the pairwise interactions between neurons is generated according to a Stochastic Block Model (SBM) with communities C_1 and C_2 . To distinguish this random case from the fixed case discussed in Chapter 3, we denote the random interaction matrix by Θ . More precisely, the entries $(\Theta_{ij})_{1 \leq i, j \leq N}$ are independent Bernoulli random variables with parameter p or q , depending on whether the corresponding edge is intra- or inter-community, respectively.

We also assume that the matrix determining whether an edge is inhibitory or excitatory - denoted by H (to distinguish it from the fixed case η in Chapter 3) - has independent and identically distributed entries, independent of Θ , with the distribution

$$H_{ij} = \begin{cases} 1 & \text{with probability } \beta, \\ -1 & \text{with probability } 1 - \beta, \end{cases} \quad (4.1)$$

where we assume $\beta \neq 1/2$.

We further assume that the community sizes are proportional to the total number of neurons: $|C_1| = \alpha_1 N$ and $|C_2| = \alpha_2 N$, with $\alpha_1 + \alpha_2 = 1$. Consequently, in addition to the parameters λ , μ_{\sim} , $\mu_{\not\sim}$, and N , the NFC in this random environment also depends on p , q , β , and α_1 . Henceforth, we denote by $\mathbb{P}_{p,q,\beta}$ the distribution of the interaction graph and by $\mathbb{E}_{p,q,\beta}$ the corresponding expectation. Moreover, for any $\theta \in \{0, 1\}^{\binom{N}{2}}$ and $\eta \in \{-1, 1\}^{\binom{N}{2}}$, we denote by $\mathbb{P}_{(\theta,\eta)}$ the stationary distribution of the process $\{X_t\}_{t \geq 0}$ and by $p_{(\theta,\eta),i}$ (for $i \in [N]$) the firing probability of neuron i ,

conditioned on the realization $\Theta = \theta$ and $H = \eta$.

Finally, we denote by $\mathbb{P}_{(\Theta, H)}$ the distribution of $\{X_t\}_{t \geq 0}$ when conditioning on the random variables Θ and H rather than on specific realizations.

Let Ω^{adm} be the set of all realizations of the random environment for which the NFC is well-defined,

$$\Omega^{adm} = \left\{ (\theta, \eta) \in \{0, 1\}^{\binom{N}{2}} \times \{-1, 1\}^{\binom{N}{2}} : p_{(\theta, \eta), i}(x) \in (0, 1) \right. \\ \left. \text{for all } x \in \{0, 1\}^N \text{ and } i \in [N] \right\}, \quad (4.2)$$

that is, for which all firing probabilities are strictly between 0 and 1. To ensure that the model is well defined even for pairs $(\theta, \eta) \notin \Omega^{adm}$, one may consider the truncated transition probabilities $(p_{(\theta, \eta), i}(x))^+ \wedge 1$, where $(\cdot)^+$ denotes the positive part, i.e., $(x)^+ = \max\{x, 0\}$. However, the following lemma shows that the random environment (Θ, H) belongs to the set of admissible realizations Ω^{adm} with high probability whenever

$$M < \lambda < 1 - M, \quad (4.3)$$

with $M = \max\{\mu_{\sim} \alpha_1 p + \mu_{\not\sim} \alpha_2 q, \mu_{\sim} \alpha_2 p + \mu_{\not\sim} \alpha_1 q\}$.

Lemma 4.1. *Suppose that (4.3) is satisfied. Then there exists a positive constant c , depending on the parameters λ , α_1 , μ_{\sim} , $\mu_{\not\sim}$, p and q , such that $\mathbb{P}_{p, q, \beta}((\Theta, H) \in \Omega^{adm}) \geq 1 - 2Ne^{-cN}$.*

The proof of Lemma 4.1 follows from a concentration of measure arguments and is presented in (COELHO *et al.*, 2025). Note that for (4.3) to hold, it is necessary that $M < 1/2$.

4.1 Mean-field Approximations

We now provide approximations for the firing mean and the synchronous firing covariance in this random environment. The proofs presented below are sketches and intended to offer an intuitive demonstration of how these statistics behave as N increases. Please refer to Appendix A for rigorous and formal proofs.

We have the following approximations under a mean-field approximation as $N \rightarrow \infty$. If $i \in C_1$:

$$\begin{cases} \sum_{j \in C_1} A_{ij}^\top & \approx (2\beta - 1) \alpha_1 \mu_{\sim} p =: g_{11}, \\ \sum_{j \in C_2} A_{ij}^\top & \approx (2\beta - 1) \alpha_2 \mu_{\not\sim} q =: g_{12}. \end{cases}$$

Similarly, if $i \in C_2$:

$$\begin{cases} \sum_{j \in C_1} A_{ij}^\top & \approx (2\beta - 1) \alpha_1 \mu_{\not\sim} q =: g_{21}, \\ \sum_{j \in C_2} A_{ij}^\top & \approx (2\beta - 1) \alpha_2 \mu_{\sim} p =: g_{22}. \end{cases}$$

The factor $2\beta - 1$ arises from the average effect of excitatory versus inhibitory connections.

Define the matrix

$$\mathcal{G} = \begin{bmatrix} g_{11} & g_{12} \\ g_{21} & g_{22} \end{bmatrix} = (2\beta - 1) \begin{bmatrix} p\mu_{\sim}\alpha_1 & q\mu_{\not\sim}\alpha_2 \\ q\mu_{\not\sim}\alpha_1 & p\mu_{\sim}\alpha_2 \end{bmatrix}. \quad (4.4)$$

Lemma 4.2. *Let \mathcal{G} be defined as in (4.4). Then, for all $z \geq 1$ and every $i \in [N]$,*

$$\left((A^\top)^z \mathbf{1}_N \right)_i \approx \mathcal{G}^z \begin{pmatrix} 1 \\ 1 \end{pmatrix} \cdot \left[\begin{pmatrix} 1 \\ 0 \end{pmatrix} \mathbf{1}_{\{i \in C_1\}} + \begin{pmatrix} 0 \\ 1 \end{pmatrix} \mathbf{1}_{\{i \in C_2\}} \right],$$

where $u \cdot v$ denotes the inner product between vector u and v .

Proof. We prove the claim by induction on z . For the base case $z = 2$, note that

$$\begin{aligned} \left((A^\top)^2 \mathbf{1}_N \right)_i &= \sum_{j=1}^N \left((A^\top)^2 \right)_{ij} = \sum_{j=1}^N \sum_{l=1}^N A_{il}^\top A_{lj}^\top = \sum_{l=1}^N A_{il}^\top \sum_{j=1}^N A_{lj}^\top \\ &\stackrel{(*)}{=} \sum_{l \sim i} A_{il}^\top (A^\top \mathbf{1}_N)_l + \sum_{l \not\sim i} A_{il}^\top (A^\top \mathbf{1}_N)_l. \end{aligned}$$

In (*), we separate the sum over l according to whether l belongs to the same community as i or not. We then obtain the desired result by using the definitions of g_{11} , g_{12} , g_{21} , and g_{22} . In particular, if $i \in C_1$, one finds that

$$\begin{aligned} \left((A^\top)^2 \mathbf{1}_N \right)_i &\approx \sum_{l \sim i} A_{il}^\top (g_{11} + g_{12}) + \sum_{l \not\sim i} A_{il}^\top (g_{21} + g_{22}) \\ &= g_{11} (g_{11} + g_{12}) + g_{12} (g_{21} + g_{22}), \end{aligned}$$

which coincides with the first entry of $\mathcal{G}^2 \begin{pmatrix} 1 \\ 1 \end{pmatrix}$. A similar calculation applies for $i \in C_2$:

$$\begin{aligned} \left((A^\top)^2 \mathbf{1}_N \right)_i &= \sum_{l \sim i} A_{il}^\top (g_{21} + g_{22}) + \sum_{l \not\sim i} A_{il}^\top (g_{11} + g_{12}) \\ &= g_{22} (g_{21} + g_{22}) + g_{21} (g_{11} + g_{12}). \end{aligned}$$

For the induction step, assume the claim is valid for $z - 1$. Then,

$$\begin{aligned}
((A^\top)^z \mathbf{1}_N)_i &= \sum_{j=1}^N ((A^\top)^z)_{ij} = \sum_{j=1}^N \sum_{l=1}^N A_{il}^\top ((A^\top)^{z-1})_{lj} \\
&= \sum_{l=1}^N A_{il}^\top \sum_{j=1}^N ((A^\top)^{z-1})_{lj} \\
&= \sum_{l=1}^N A_{il}^\top ((A^\top)^{z-1} \mathbf{1}_N)_l \\
&= \sum_{l \sim i} A_{il}^\top ((A^\top)^{z-1} \mathbf{1}_N)_l + \sum_{l \not\sim i} A_{il}^\top ((A^\top)^{z-1} \mathbf{1}_N)_l,
\end{aligned}$$

where the summation is again split according to the community membership of l .

Denoting $\mathcal{G}^{z-1} = \begin{bmatrix} a & b \\ c & d \end{bmatrix}$, if $i \in C_1$,

$$\begin{aligned}
((A^\top)^z \mathbf{1}_N)_i &\approx g_{11} \mathcal{G}^{z-1} \begin{pmatrix} 1 \\ 1 \end{pmatrix} \cdot \begin{pmatrix} 1 \\ 0 \end{pmatrix} + g_{12} \mathcal{G}^{z-1} \begin{pmatrix} 1 \\ 1 \end{pmatrix} \cdot \begin{pmatrix} 0 \\ 1 \end{pmatrix} \\
&= g_{11} (a + b) + g_{12} (c + d),
\end{aligned}$$

which is exactly the first entry of $\mathcal{G} \mathcal{G}^{z-1} \begin{pmatrix} 1 \\ 1 \end{pmatrix} = \mathcal{G}^z \begin{pmatrix} 1 \\ 1 \end{pmatrix}$. Analogously, if $i \in C_2$, one obtains that

$$\begin{aligned}
((A^\top)^z \mathbf{1}_N)_i &\approx g_{22} \mathcal{G}^{z-1} \begin{pmatrix} 1 \\ 1 \end{pmatrix} \cdot \begin{pmatrix} 0 \\ 1 \end{pmatrix} + g_{21} \mathcal{G}^{z-1} \begin{pmatrix} 1 \\ 1 \end{pmatrix} \cdot \begin{pmatrix} 1 \\ 0 \end{pmatrix} \\
&= g_{22} (c + d) + g_{21} (a + b),
\end{aligned}$$

which coincides with the second entry of $\mathcal{G}^z \begin{pmatrix} 1 \\ 1 \end{pmatrix}$.

This step completes the induction and proves the lemma. \square

With Lemma 4.2 in hand and supposing that condition (4.3) holds, we can show that the average firing probability of neuron i , namely, $\mathbb{E}_{p,q,\beta} [\mathbb{P}_{(\Theta,H)} (X_{i,0} = 1)]$, converges (as $N \rightarrow \infty$) to one of two possible values, m_1 or m_2 , depending only on whether $i \in C_1$ or $i \in C_2$, respectively.

Since (4.3) holds, Lemma 4.1 assures that we are working in the set of admissible realizations Ω^{adm} with high probability, and then we can use the result from Theorem 3.1.

For instance, if $i \in C_1$, we have from (3.5) that

$$\begin{aligned} m_i &= \lambda \sum_{z=0}^{\infty} ((A^\top)^z \mathbf{1}_N)_i \approx \lambda \sum_{z=0}^{\infty} \mathcal{G}^z \begin{pmatrix} 1 \\ 1 \end{pmatrix} \cdot \begin{pmatrix} 1 \\ 0 \end{pmatrix} \\ &= \lambda (I - \mathcal{G})^{-1} \begin{pmatrix} 1 \\ 1 \end{pmatrix} \cdot \begin{pmatrix} 1 \\ 0 \end{pmatrix} \\ &= \lambda \frac{1 - g_{22} + g_{12}}{(1 - g_{11})(1 - g_{22}) - g_{12}g_{21}} =: m_1. \end{aligned}$$

Similarly, if $i \in C_2$:

$$\begin{aligned} m_i &= \lambda \sum_{z=0}^{\infty} ((A^\top)^z \mathbf{1}_N)_i \approx \lambda \sum_{z=0}^{\infty} \mathcal{G}^z \begin{pmatrix} 1 \\ 1 \end{pmatrix} \cdot \begin{pmatrix} 0 \\ 1 \end{pmatrix} \\ &= \lambda (I - \mathcal{G})^{-1} \begin{pmatrix} 1 \\ 1 \end{pmatrix} \cdot \begin{pmatrix} 0 \\ 1 \end{pmatrix} \\ &= \lambda \frac{1 - g_{11} + g_{21}}{(1 - g_{11})(1 - g_{22}) - g_{12}g_{21}} =: m_2. \end{aligned}$$

When $\alpha_1 \neq \alpha_2$, we have that $m_1 \neq m_2$. Hence, for unbalanced networks, the entries from the vector of firing mean spiking activities have two different values, m_1 and m_2 , which carry information that may help in community separation as $N \rightarrow \infty$.

Now, in the special case where $\alpha_1 = \alpha_2 = 1/2$, the firing means coincide for both communities:

$$m_i \approx \lambda \frac{(1 + \frac{1}{2}(2\beta - 1)(\mu_{\not\sim} q - \mu_{\sim} p))}{1 - (2\beta - 1)\mu_{\sim} p + \frac{1}{4}(2\beta - 1)^2(\mu_{\sim}^2 p^2 - \mu_{\not\sim}^2 q^2)} =: m^*.$$

Consequently, the firing variance is also equal for all neurons:

$$v^* = m^* (1 - m^*).$$

Under these circumstances, the firing mean vector does not hint at the underlying graph's community structure. So, let us turn our attention to the synchronous firing covariance. In what follows, we consider here only the special case in which $\alpha_1 = \alpha_2 = 1/2$.

Note that, in this special case, $g_{11} = g_{22} =: g_{\sim}$, and $g_{12} = g_{21} =: g_{\not\sim}$. We now provide the asymptotic values for the entries of $\Sigma^{(0)}$. When $i = j$, $\Sigma_{ij}^{(0)}$ is given by v^* , and thus, what remains to be found are the off-diagonal entries of the synchronous covariance matrix.

Lemma 4.3. *Let \mathcal{G} be defined as in (4.4). If $\alpha_1 = \alpha_2 = 1/2$, then for all $z \geq 1$ and*

$(i, j) \in [N]^2$, with $i \neq j$, the following is true:

$$(L^z \text{vec}(\text{diag}(v)))_s \approx \frac{2v^*}{N} (\mathcal{G}^{2z})_{ab},$$

where, $s = N(i-1) + j$ and $(i, j) \in C_a \times C_b$, with $a, b \in \{1, 2\}$.

Proof. We prove the claim by induction on z . For the base case $z = 1$, note that

$$(L \text{vec}(\text{diag}(v)))_s = \sum_{u=1}^{N^2} L_{su} \text{vec}(\text{diag}(v))_u.$$

By the definitions of L and $\text{vec}(\text{diag}(v))$, we have

$$(L \text{vec}(\text{diag}(v)))_s = \sum_{(k,l) \in [N]^2} A_{ik}^\top A_{jl}^\top \text{diag}(v)_{kl}.$$

Since $\text{diag}(v)_{kl} = v^*$ when $k = l$ and zero otherwise, it follows that

$$\begin{aligned} (L \text{vec}(\text{diag}(v)))_s &= \sum_{k \in [N]} A_{ik}^\top A_{jk}^\top (\text{diag}(v))_{kk} \\ &\approx v^* \sum_{k \in [N]} A_{ik}^\top A_{jk}^\top. \end{aligned}$$

By the mean-field approximations of A^\top , we obtain

$$\sum_{k \in [N]} A_{ik}^\top A_{jk}^\top \approx \frac{1}{2} \frac{1}{N} \begin{cases} (p\mu_{\sim}(2\beta-1))^2 + (q\mu_{\not\sim}(2\beta-1))^2 & \text{if } i \sim j, \\ 2(p\mu_{\sim}(2\beta-1))(q\mu_{\not\sim}(2\beta-1)) & \text{if } i \not\sim j, \end{cases}$$

or equivalently,

$$\sum_{k \in [N]} A_{ik}^\top A_{jk}^\top \approx \frac{2}{N} \begin{cases} g_{\sim}^2 + g_{\not\sim}^2 & \text{if } i \sim j, \\ 2g_{\sim}g_{\not\sim} & \text{if } i \not\sim j. \end{cases}$$

Note that, when $\alpha_1 = \alpha_2 = 1/2$,

$$\mathcal{G}^2 = \begin{bmatrix} g_{\sim}^2 + g_{\not\sim}^2 & 2g_{\sim}g_{\not\sim} \\ 2g_{\sim}g_{\not\sim} & g_{\sim}^2 + g_{\not\sim}^2 \end{bmatrix}.$$

Hence, the base case is established:

$$(L \text{vec}(\text{diag}(v)))_s \approx \frac{2v^*}{N} (\mathcal{G}^2)_{ab}.$$

For the induction step, assume the claim holds for $z - 1$. Then,

$$\begin{aligned} (L^z \text{vec}(\text{diag}(v)))_s &= \sum_{u=1}^{N^2} L_{su} (L^{z-1} \text{vec}(\text{diag}(v)))_u \\ &= \sum_{k,l=1}^N A_{ik}^\top A_{jl}^\top (L^{z-1} \text{vec}(\text{diag}(v)))_{N(k-1)+l}. \end{aligned}$$

By the induction hypothesis, if $(k, l) \in C_c \times C_d$ (with $c, d \in \{1, 2\}$) then

$$(L^{z-1} \text{vec}(\text{diag}(v)))_{N(k-1)+l} \approx \frac{2v^*}{N} (\mathcal{G}^{2(z-1)})_{cd}$$

Thus,

$$\begin{aligned} (L^z \text{vec}(\text{diag}(v)))_s &\approx \frac{2v^*}{N} \sum_{c=1}^2 \sum_{d=1}^2 (\mathcal{G}^{2(z-1)})_{cd} \sum_{k \in C_c} \sum_{l \in C_d} A_{ik}^\top A_{jl}^\top \\ &= \frac{2v^*}{N} \sum_{c=1}^2 \sum_{d=1}^2 (\mathcal{G}^{2(z-1)})_{cd} \sum_{k \in C_c} A_{ik}^\top \sum_{l \in C_d} A_{jl}^\top \end{aligned}$$

Recall that $(i, j) \in C_a \times C_b$. Then

$$\sum_{k \in C_c} A_{ik}^\top \approx \begin{cases} g_{\sim} & \text{if } a = c, \\ g_{\not\sim} & \text{if } a \neq c; \end{cases}$$

and similarly,

$$\sum_{l \in C_d} A_{jl}^\top \approx \begin{cases} g_{\sim} & \text{if } b = d, \\ g_{\not\sim} & \text{if } b \neq d. \end{cases}$$

Now, consider $(i, j) \in C_1 \times C_1$. Then,

$$\begin{aligned} (L^z \text{vec}(\text{diag}(v)))_s &\approx \frac{2v^*}{N} [(\mathcal{G}^{2(z-1)})_{11} g_{\sim}^2 + (\mathcal{G}^{2(z-1)})_{12} g_{\sim} g_{\not\sim} + \\ &\quad + (\mathcal{G}^{2(z-1)})_{21} g_{\sim} g_{\not\sim} + (\mathcal{G}^{2(z-1)})_{22} g_{\not\sim}^2] \\ &= \frac{2v^*}{N} [(\mathcal{G}^{2(z-1)})_{11} (g_{\sim}^2 + g_{\not\sim}^2) + (\mathcal{G}^{2(z-1)})_{12} (2g_{\sim} g_{\not\sim})] \\ &= \frac{2v^*}{N} (\mathcal{G}^{2(z-1)} \mathcal{G}^2)_{11} \\ &= \frac{2v^*}{N} (\mathcal{G}^{2z})_{11}. \end{aligned}$$

The other cases can be handled analogously.

This step completes the induction and proves the lemma. \square

Using the result of Lemma 4.3 and supposing again that condition (4.3) holds,

we can write the off-diagonal entries of the synchronous firing covariance $\Sigma^{(0)}$ as

$$\begin{aligned}
\Sigma_{ij}^{(0)} &= \text{vec}(\Sigma^{(0)})_s \\
&\stackrel{(*)}{=} \sum_{z=0}^{\infty} (L^z \text{vec}(\text{diag}(v)))_s \\
&= \text{diag}(v)_{ij} + \sum_{z=1}^{\infty} (L^z \text{vec}(\text{diag}(v)))_s \\
&= \sum_{z=1}^{\infty} (L^z \text{vec}(\text{diag}(v)))_s \\
&\approx \frac{2v^*}{N} \sum_{z=1}^{\infty} (\mathcal{G}^{2z})_{ab} \\
&= \frac{2v^*}{N} \left(\sum_{z=1}^{\infty} \mathcal{G}^{2z} \right)_{ab} \\
&= \frac{2v^*}{N} \left((\mathbf{I}_{N^2} - \mathcal{G}^2)^{-1} - \mathbf{I}_{N^2} \right)_{ab},
\end{aligned}$$

where $s = N(i-1) + j$ and $(i, j) \in C_a \times C_b$, for $i \neq j$. The equality in $(*)$ holds with high probability if (4.3) holds.

This result indicates that in the limit, as $N \rightarrow \infty$, the synchronous firing covariance takes only two possible values depending solely on whether the neurons belong to the same community or different communities. So, although the firing mean vector is not indicative of community membership when $\alpha_1 = \alpha_2 = 1/2$, the synchronous firing covariance could lead us to this information.

4.2 Validation of Mean-Field Approximations Against Theoretical Results

Section 4.1 presented asymptotic expressions for certain statistics in large random networks. In Figure 4.1, we plot the absolute error between the average mean firing rate - computed over all neurons in a community - and the corresponding asymptotic mean firing rate for that community as a function of N . The figure on the left presents the case where $\alpha_1 \neq \alpha_2$, while the figure on the right depicts the balanced case ($\alpha_1 = \alpha_2$). Note that, for balanced networks, the asymptotic mean firing rate is identical for both communities, and it is not possible to separate neurons in communities based on this attribute. Therefore, it is natural that the errors for both communities coincide. However, for the same case, the asymptotic mean covariance distinguishes between intra- and inter-community neuron pairs, providing information on whether two neurons belong to the same community.

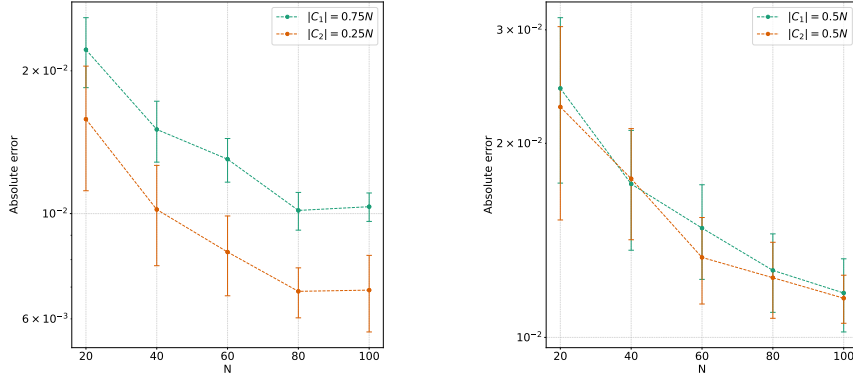


Figure 4.1: Absolute error between theoretical firing mean and the corresponding asymptotic firing mean. The left figure shows the unbalanced case while the right figure shows the balanced case ($\alpha_1 = \alpha_2$). Model parameters: $\lambda = 0.25$, $\beta = 0.6$, $p = 0.3$, $q = 0.15$, $\mu_{\neq} = \mu_{\sim}/2$, $\mu_{\sim} = 1.02$ (left figure) and $\mu_{\sim} = 1.33$ (right figure). For each N , 10 networks were generated, and the average error and one standard deviation are shown.

Figure 4.2 presents a similar error analysis for the covariance. It shows the absolute error between the average covariance (computed over all pairs of neurons within the same community and across different communities) and the respective asymptotic mean covariance, again as a function of N , for a balanced network. In both cases - mean firing and synchronous firing covariance - the error decreases as N increases, confirming our asymptotic approximations' accuracy in the large-network limit. In particular, the error for the intra-community covariance is more prominent in absolute value, likely due to its higher magnitude relative to the inter-community covariance.

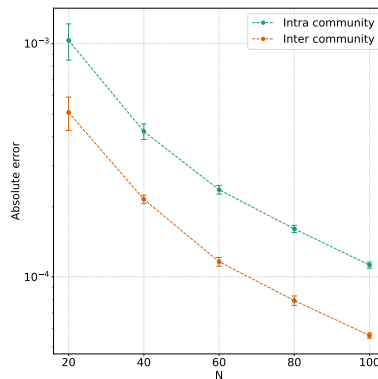


Figure 4.2: Absolute error between theoretical synchronous firing covariance and the corresponding asymptotic firing covariance. Model parameters: $\lambda = 0.25$, $\beta = 0.6$, $p = 0.3$, $q = 0.15$, $\mu_{\neq} = \mu_{\sim}/2$, $\mu_{\sim} = 1.33$. For each N , 10 networks were generated, and the average error and one standard deviation are shown.

Chapter 5

Conclusion

This dissertation introduced a simple network model comprising two communities and edge types (excitatory or inhibitory) alongside a linear neuronal firing model grounded on neuroscience principles to represent the structural brain network and neuronal firing dynamics. A rigorous mathematical analysis of the model yielded closed-form expressions for the firing mean and pairwise spike train covariances (synchronous and one-lagged). For a fixed environment, we obtain exact statistics expressions for each neuron, while for random environments we obtain asymptotic expressions relating to the neuron’s community membership. These expressions elucidate the dependencies of these statistics on model parameters, including the proportion of neurons in each community, the rate of excitatory and inhibitory connections, and interaction strengths.

For a fixed environment, theoretical derivations established expressions for each neuron’s firing mean and firing covariances for synchronous and one-lagged series. The covariance pattern revealed an insightful result: in the synchronous case, neurons sharing common neighbours exhibit higher covariance values (in magnitude), whereas in the one-lagged case, elevated covariance is observed between directly connected neurons. This outcome aligns with the model assumptions, where a neuron’s firing only influences the firing probability of its neighbours in the subsequent time step. Neurons with more shared neighbours receive similar contributions within the same time step. Interestingly, the two covariances provide complementary information concerning the structure of the underlying network.

Empirical experiments validated these theoretical findings. Based on the proposed model, spike train series generated by a stochastic computer simulator were used to compute numerical estimates of firing rates and pairwise correlations. These were then compared with the analytically derived expressions. The absolute error between the empirical and theoretical values decreases proportionally to \sqrt{T} (where T is the time series length). It remains almost unaffected by model parameters, demonstrating the robustness of the analytical expressions that have been derived.

The primary factor of numerical accuracy is the spike train length.

For the random environment, asymptotic expressions were obtained through proof sketches based on mean-field approximations. However, formal proofs of such results have also been derived (see Appendix A). Comparisons with statistics from real networks indicate that the error goes to zero as $N \rightarrow \infty$ but also that the values converge to a constant if multiplied by N . The asymptotic firing mean converges to two distinct values determined solely by the neuron’s community membership. In the balanced case, where both communities are of equal size, these values coincide. However, in this scenario, synchronous covariances converge only to two values depending on whether the neurons belong to the same or different communities. These dependencies suggest that community structure can be inferred solely from observed firing statistics, independent of prior knowledge of model parameters. Indeed, related work has tackled this problem of detecting the two communities from the empirical covariance measured on simulated data (COELHO *et al.*, 2025).

5.1 Future Work

Several avenues remain open for further exploration of this neuronal activity model. A natural extension involves considering more than two communities: How do the expressions for firing mean and covariance change under this scenario? Can they still be leveraged to distinguish communities? Addressing these questions would contribute to developing a more general model applicable to realistic settings with multiple interacting communities.

A deeper investigation into the theoretical foundations of community recovery based on model parameter separation is also warranted. AVRACHENKOV *et al.* (2022) provided several proofs in the context of the Stochastic Block Model for non-binary networks and temporal networks. Their methodologies could inspire similar analyses within our framework, incorporating network dynamics to enhance community detection and establishing an information-theoretic limit for exact recovery from the parameters of firing dynamics and network structure.

Recent studies have explored community recovery in scenarios where nodes exhibit overlapping memberships, meaning a single node can belong to multiple communities simultaneously (XIE *et al.*, 2013). From a biological perspective, this approach could better capture neurons involved in multiple signalling pathways, influencing distinct functions. However, accommodating this feature would require non-trivial changes to the model, potentially complicating the derivation of theoretical results. Despite these challenges, such an extension would represent a compelling research direction.

References

- SEGUIN, C., SPORNS, O., ZALESKY, A. “Brain network communication: concepts, models and applications”, *Nature Reviews Neuroscience*, v. 24, n. 9, 2023.
- LYNN, C. W., BASSETT, D. S. “The physics of brain network structure, function and control”, *Nature Reviews Physics*, v. 1, n. 5, 2019.
- HERCULANO-HOUZEL, S. “The human brain in numbers: a linearly scaled-up primate brain”, *Frontiers in Human Neuroscience*, v. 3, 2009.
- KANDEL, E. R., SCHWARTZ, J. H., JESSELL, T. M., et al. *Principles of neural science*. McGraw-hill New York, 2000.
- SPORNS, O., BETZEL, R. F. “Modular brain networks”, *Annual Review of Psychology*, v. 67, 2016.
- DONNER, C., BARTRAM, J., HORNAUER, P., et al. “Ensemble learning and ground-truth validation of synaptic connectivity inferred from spike trains”, *PLOS Computational Biology*, v. 20, n. 4, 2024.
- REN, N., ITO, S., HAFIZI, H., et al. “Model-based detection of putative synaptic connections from spike recordings with latency and type constraints”, *Journal of Neurophysiology*, v. 124, n. 6, 2020.
- KORHONEN, O., ZANIN, M., PAPO, D. “Principles and open questions in functional brain network reconstruction”, *Human Brain Mapping*, v. 42, n. 11, 2021.
- KOBAYASHI, R., KURITA, S., KURTH, A., et al. “Reconstructing neuronal circuitry from parallel spike trains”, *Nature Communications*, v. 10, n. 1, 2019.
- ENDO, D., KOBAYASHI, R., BARTOLO, R., et al. “A convolutional neural network for estimating synaptic connectivity from spike trains”, *Scientific Reports*, v. 11, n. 1, 2021.

- COTMAN, C. W., MCGAUGH, J. L. *Behavioral neuroscience: An introduction*. Academic Press, 1980.
- DALE, H. “Pharmacology and Nerve-Endings”. 1935.
- ECCLES, J. C., FATT, P., KOKETSU, K. “Cholinergic and inhibitory synapses in a pathway from motor-axon collaterals to motoneurons”, *The Journal of Physiology*, v. 126, n. 3, 1954.
- ROOT, D. H., MEJIAS-APONTE, C. A., ZHANG, S., et al. “Single rodent meso-habenular axons release glutamate and GABA”, *Nature Neuroscience*, v. 17, n. 11, 2014.
- BOONSTRA, E., DE KLEIJN, R., COLZATO, L. S., et al. “Neurotransmitters as food supplements: the effects of GABA on brain and behavior”, *Frontiers in Psychology*, v. 6, 2015.
- KOH, W., KWAK, H., CHEONG, E., et al. “GABA tone regulation and its cognitive functions in the brain”, *Nature Reviews Neuroscience*, v. 24, n. 9, 2023.
- MELDRUM, B. S. “Glutamate as a Neurotransmitter in the Brain: Review of Physiology and Pathology”, *The Journal of Nutrition*, v. 130, n. 4, 2000.
- CASH, S., YUSTE, R. “Linear Summation of Excitatory Inputs by CA1 Pyramidal Neurons”, *Neuron*, v. 22, n. 2, 1999.
- BULLMORE, E., SPORNS, O. “Complex brain networks: graph theoretical analysis of structural and functional systems”, *Nature Reviews Neuroscience*, v. 10, n. 3, 2009.
- HILGETAG, C.-C., BURNS, G. A., O’NEILL, M. A., et al. “Anatomical connectivity defines the organization of clusters of cortical areas in the macaque and the cat”, *Philosophical Transactions of the Royal Society of London. Series B: Biological Sciences*, v. 355, n. 1393, 2000.
- EULER, L. “Solutio problematis ad geometriam situs pertinentis”, *Commentarii Academiae Scientiarum Imperialis Petropolitanae*, v. 8, 1736.
- ERDŐS, P., RÉNYI, A. “On random graphs I”, *Publicationes Mathematicae Debrecen*, v. 6, 1959.
- FRIEZE, A., KAROŃSKI, M. *Introduction to Random Graphs*. Cambridge University Press, 2015.

- HOLLAND, P. W., LASKEY, K. B., LEINHARDT, S. “Stochastic blockmodels: First steps”, *Social Networks*, v. 5, n. 2, 1983.
- AVRACHENKOV, K., DREVEYTON, M., LESKELÄ, L. “Community recovery in non-binary and temporal stochastic block models”. 2022. Available at: <<https://arxiv.org/abs/2008.04790>>.
- BROOKS, S., GELMAN, A., JONES, G., et al. *Handbook of Markov Chain Monte Carlo*. CRC press, 2011.
- HÄGGSTRÖM, O. *Finite Markov Chains and Algorithmic Applications*. Cambridge University Press, 2002.
- LINDERMAN, S., ADAMS, R. P., PILLOW, J. W. “Bayesian latent structure discovery from multi-neuron recordings”, *Advances in Neural Information Processing Systems (NIPS)*, v. 29, 2016.
- HUMPHRIES, M. D. “Spike-Train Communities: Finding Groups of Similar Spike Trains”, *Journal of Neuroscience*, v. 31, n. 6, 2011.
- HERZOG, R., MORALES, A., MORA, S., et al. “Scalable and accurate method for neuronal ensemble detection in spiking neural networks”, *PLOS ONE*, v. 16, n. 7, 2021.
- CHEVALLIER, J., OST, G. “Community detection for binary graphical models in high dimension”. 2024. Available at: <<https://arxiv.org/abs/2411.15627>>.
- COELHO, T., PINTO, C., OST, G., et al. “Predicting Spike Train Correlations and Neuron Clusters in Structural Brain Networks”, *Under review*, 2025.
- COELHO, T. *Clustering structural brain networks using pairwise correlations of spike trains*. Masters Thesis, Federal University of Rio de Janeiro, 2025.
- XIE, J., KELLEY, S., SZYMANSKI, B. K. “Overlapping community detection in networks: The state-of-the-art and comparative study”, *ACM Comput. Surv.*, v. 45, n. 4, 2013.
- BOUCHERON, S., LUGOSI, G., MASSART, P. *Concentration Inequalities: A Nonasymptotic Theory of Independence*. Oxford University Press, 2013.

Appendix A

Rigorous Proofs

These following proofs were extracted from COELHO *et al.* (2025).

Theorem A.1. *Suppose (4.3) is granted. Let $\mathcal{G} = \begin{pmatrix} g_{11} & g_{12} \\ g_{21} & g_{22} \end{pmatrix} = (2\beta -$*

1) $\begin{pmatrix} p\mu_{\sim\alpha_1} & q\mu_{\not\sim\alpha_2} \\ q\mu_{\not\sim\alpha_1} & p\mu_{\sim\alpha_2} \end{pmatrix}$ and define

$$m_1 = \frac{\lambda}{\det(\mathbf{I}_2 - \mathcal{G})} (1 - g_{22} + g_{12}) \text{ and } m_2 = \frac{\lambda}{\det(\mathbf{I}_2 - \mathcal{G})} (1 - g_{11} + g_{21}),$$

where \mathbf{I}_2 is the two-dimensional identity matrix. Then, there exists a positive constant K independent of N such that for all $N \geq 2$,

$$\mathbb{E}_{p,q,\beta} \left[\max_{1 \leq i \leq N} |\mathbb{P}_{(\Theta,H)}(X_{i,0} = 1) - (m_1 \mathbf{1}_{\{i \in C_1\}} + m_2 \mathbf{1}_{\{i \in C_2\}})| \right] \leq K \sqrt{\frac{\log(N)}{N}}.$$

Proof. The proof goes along Lemma 8.2 of CHEVALLIER and OST (2024), where a similar result was established in a similar framework. Throughout the proof, K denotes a positive constant independent of N that may change from one line to another. Let $Q = (\mathbf{I}_N - A^\top)^{-1}$ and define the following random vectors: $Q\mathbf{1}_N = \ell$, $A^\top \mathbf{1}_{C_i} = C^{(i)}$ and $Q\mathbf{1}_{C_i} = \ell^{(i)}$ for $i = 1, 2$, where, $\mathbf{1}_N$ (resp., $\mathbf{1}_{C_i}$) denotes the column vector of length N with all entries equal to 1 (resp., all entries in C_i equal to 1 and 0 otherwise). With this notation, first, observe that we can write $\ell = \ell^{(1)} + \ell^{(2)}$ and $\ell^{(i)} = \mathbf{1}_{C_i} + QC^{(i)}$ for $i = 1, 2$. Next, introducing the vectors $\epsilon^{(1)} = C^{(1)} - (g_{11}\mathbf{1}_{C_1} + g_{21}\mathbf{1}_{C_2})$ and $\epsilon^{(2)} = C^{(2)} - (g_{22}\mathbf{1}_{C_2} + g_{12}\mathbf{1}_{C_1})$, we then deduce that $\ell^{(1)} = \mathbf{1}_{C_1} + Q\epsilon^{(1)} + g_{11}\ell^{(1)} + g_{21}\ell^{(2)}$ and $\ell^{(2)} = \mathbf{1}_{C_2} + Q\epsilon^{(2)} + g_{12}\ell^{(1)} + g_{22}\ell^{(2)}$. As a consequence, we can write

$$\ell^{(1)} = \frac{1}{1 - g_{11}} \mathbf{1}_{C_1} + \frac{1}{1 - g_{11}} Q\epsilon^{(1)} + \frac{g_{21}}{1 - g_{11}} \ell^{(2)}, \quad (\text{A.1})$$

and

$$\frac{\det(\mathbf{I}_2 - \mathcal{G})}{1 - g_{11}} \ell^{(2)} = \mathbf{1}_{C_2} + Q\epsilon^{(2)} + \frac{g_{12}}{1 - g_{11}} \mathbf{1}_{C_1} + \frac{g_{12}}{1 - g_{11}} Q\epsilon^{(1)}. \quad (\text{A.2})$$

Now, using the fact that the coordinates of the vectors $\epsilon^{(1)}$ and $\epsilon^{(2)}$ are subgaussian random variables with parameter $\max\{\mu_{\sim}^2, \mu_{\not\sim}^2\}/N$, and defining $\|\epsilon^{(i)}\|_{\infty} := \max_{\ell \in [N]} |\epsilon_{\ell}^{(i)}|$, we can show from the maximal inequality for subgaussian random variables (see (BOUCHERON *et al.*, 2013, Theorem 2.5)) that

$$\mathbb{E}_{p,q,\beta} [\|\epsilon^{(i)}\|_{\infty}] \leq K \sqrt{\frac{\log(N)}{N}},$$

for some constant K not depending on N . Combining the above inequality with (A.2), we can show that

$$\mathbb{E}_{p,q,\beta} \left[\left\| \ell^{(2)} - \frac{1}{\det(\mathbf{I}_2 - \mathcal{G})} (g_{12} \mathbf{1}_{C_1} + (1 - g_{11}) \mathbf{1}_{C_2}) \right\|_{\infty} \right] \leq K \sqrt{\frac{\log(N)}{N}}.$$

Then, using the above inequality, the bound on the sup-norm of the random vector $\epsilon^{(1)}$ and identity (A.1), one can deduce that

$$\mathbb{E}_{p,q,\beta} \left[\left\| \ell^{(1)} - \frac{1}{\det(\mathbf{I}_2 - \mathcal{G})} ((1 - g_{22}) \mathbf{1}_{C_1} + g_{21} \mathbf{1}_{C_2}) \right\|_{\infty} \right] \leq K \sqrt{\frac{\log(N)}{N}}.$$

Recalling that $\ell = \ell^{(1)} + \ell^{(2)}$, we obtain from the above estimates that

$$\mathbb{E}_{p,q,\beta} \left[\left\| \ell - \left(\frac{(1 - g_{22} + g_{12})}{\det(\mathbf{I}_2 - \mathcal{G})} \mathbf{1}_{C_1} + \frac{(1 - g_{11} + g_{21})}{\det(\mathbf{I}_2 - \mathcal{G})} \mathbf{1}_{C_2} \right) \right\|_{\infty} \right] \leq K \sqrt{\frac{\log(N)}{N}}. \quad (\text{A.3})$$

Now, observe that Theorem 3.1 implies that, on the event $\{(\Theta, H) \in \Omega^{adm}\}$, we can write $m = \lambda \ell$ so that by triangle inequality we obtain that

$$\begin{aligned} \mathbb{E}_{p,q,\beta} \left[\left\| m - (m_1 \mathbf{1}_{C_1} + m_2 \mathbf{1}_{C_2}) \right\|_{\infty} \right] &\leq 2\mathbb{P}_{p,q,\beta}((\Theta, H) \notin \Omega^{adm}) \\ &\quad + \lambda \mathbb{E}_{p,q,\beta} \left[\left\| \ell - \left(\frac{(1 - g_{22} + g_{12})}{\det(\mathbf{I}_2 - \mathcal{G})} \mathbf{1}_{C_1} + \frac{(1 - g_{11} + g_{21})}{\det(\mathbf{I}_2 - \mathcal{G})} \mathbf{1}_{C_2} \right) \right\|_{\infty} \right]. \end{aligned}$$

Finally, using Lemma 4.1 and (A.3), the result follows. \square

Theorem A.2. *Assume that $\alpha_1 = \alpha_2$ and suppose (4.3) is granted. Let $\mathcal{G} = \frac{(2\beta-1)}{2} \begin{pmatrix} p\mu_{\sim}\alpha_1 & q\mu_{\not\sim}\alpha_2 \\ q\mu_{\not\sim}\alpha_1 & p\mu_{\sim}\alpha_2 \end{pmatrix}$ and define*

$$m = \frac{\lambda}{\det(\mathbf{I}_2 - \mathcal{G})} (1 - p\mu_{\sim} + q\mu_{\not\sim}),$$

$$g_{\sim} = ((\mathbf{I}_2 - \mathcal{G}^2)^{-1} - \mathbf{I}_2)_{11},$$

and

$$g_{\neq} = ((\mathbf{I}_2 - \mathcal{G}^2)^{-1} - \mathbf{I}_2)_{12},$$

where \mathbf{I}_2 is the two dimensional identity matrix.

Then, there exists a positive constant K , independent of N , such that for all $N \geq 2$,

$$\mathbb{E}_{p,q,\beta} \left[\max_{1 \leq i \neq j \leq N} \left| \Sigma_{ij}^{(0)} - \frac{2m(1-m)}{N} (g_{\sim} \mathbf{1}_{\{i \sim j\}} + g_{\neq} \mathbf{1}_{\{i \neq j\}}) \right| \right] \leq K \sqrt{\frac{\log(N)}{N^3}}.$$

Proof. The proof is similar to Proposition 4.2 of CHEVALLIER and OST (2024).

Throughout the proof, K denotes a positive constant independent of N that may change from line to line. Moreover, $\|\cdot\|_{\infty}$ will denote the maximum norm of vectors, whereas $\|\cdot\|_{\infty}$ the maximum norm of matrices. Let us first rewrite the claim in a vectorized form. To do that, let us define the following N^2 -dimensional vectors: $a_{\sim} = \text{vec}(\mathbf{1}_{C_1} \mathbf{1}_{C_1}^T + \mathbf{1}_{C_2} \mathbf{1}_{C_2}^T - I_N)$ and $a_{\neq} = \text{vec}(\mathbf{1}_N \mathbf{1}_N^T - \mathbf{1}_{C_1} \mathbf{1}_{C_1}^T - \mathbf{1}_{C_2} \mathbf{1}_{C_2}^T)$, where $\mathbf{1}_N$ (resp., $\mathbf{1}_{C_i}$) denotes the column vector of length N with all entries equal to 1 (resp., all entries in C_i equal to 1 and 0 otherwise). The claim can then be rewritten as

$$\mathbb{E}_{p,q,\beta} \left[\left\| \text{vec}(\Sigma^{(0)}) - \text{vec}(\text{diag}(v)) - \frac{2m(1-m)}{N} (g_{\sim} a_{\sim} + g_{\neq} a_{\neq}) \right\|_{\infty} \right] \leq K \sqrt{\frac{\log(N)}{N^3}},$$

where $v = (v_1, \dots, v_N)^T$ and $v_i = m_i(1 - m_i)$ is the firing variance of $i \in [N]$ in the random environment (Θ, H) (here $m_i = \mathbb{P}_{(\Theta, H)}(X_{i,0} = 1)$). Now, by Corollary 3.2.1, on the event $\{(\Theta, H) \in \Omega^{adm}\}$, we can write $\text{vec}(\Sigma^{(0)}) = \sum_{k=0}^{\infty} L^k \text{vec}(\text{diag}(v))$. Thus, by triangle inequality together with the fact that $\left\| \text{vec}(\Sigma^{(0)}) - \text{vec}(\text{diag}(v)) - \frac{2m(1-m)}{N} (g_{\sim} a_{\sim} + g_{\neq} a_{\neq}) \right\|_{\infty}$ is bounded and using Lemma 4.1, it suffices to show that

$$\mathbb{E}_{p,q,\beta} \left[\left\| \sum_{k=1}^{\infty} L^k \text{vec}(\text{diag}(v)) - \frac{2m(1-m)}{N} (g_{\sim} a_{\sim} + g_{\neq} a_{\neq}) \right\|_{\infty} \right] \leq K \sqrt{\frac{\log(N)}{N^3}}.$$

To show the above estimate, we start dealing with the first term $L \text{vec}(\text{diag}(v))$. Recall, from Section 3.2, that the vectorization $\text{vec}(M)$ of a $N \times N$ matrix M is a N^2 -dimensional vector having value M_{ij} in its k -th coordinate where $k = i + (j-1)N$. In the rest of the proof, with a slight abuse of notation, we will write $\text{vec}(M)_{ij}$ to denote the coordinate $k = i + (j-1)N$ of the vector $\text{vec}(M)$. By employing a similar abuse of notation, we will write $(A \otimes B)_{ij,kl}$ to denote the entry $(u, v) = (N(i-1) + j, N(k-1) + \ell)$ of the $N^2 \times N^2$ matrix $A \otimes B$ obtained as the Kronecker product between the matrices A and B . With this notation, take $i, j \in [N]$ and

observe that we can write

$$(L \operatorname{vec}(\operatorname{diag}(v)))_{ij} = \sum_{(k,\ell) \in [N]^2} L_{ij,k\ell} (\operatorname{vec}(\operatorname{diag}(v)))_{k\ell} = \mathbf{1}_{\{i \neq j\}} \sum_{k=1}^N A_{ki} A_{kj} m_k (1 - m_k),$$

where, in the second equality, we have used the definition of the $N^2 \times N^2$ matrix L and of the vector of variances v . Next, introducing the random variables

$$S_{ij}^{(r)} = \frac{1}{N} \sum_{k \in C_r} \theta_{ki} \theta_{jj} \eta_{ki} \eta_{kj} m_k (1 - m_k), i \neq j, r \in \{1, 2\},$$

and using the definition of the matrix A (recall (3.3)), we deduce that

$$\begin{aligned} (L \operatorname{vec}(\operatorname{diag}(v)))_{ij} &= N^{-1} \mathbf{1}_{\{i \neq j\}} \left[\mathbf{1}_{\{i \neq j\}} \mu_{\neq} (S_{ij}^{(1)} + S_{ij}^{(2)}) \right. \\ &\quad \left. + \mathbf{1}_{\{i,j \in C_1\}} \left((\mu_{\sim})^2 S_{ij}^{(1)} + (\mu_{\neq})^2 S_{ij}^{(2)} \right) + \mathbf{1}_{\{i,j \in C_2\}} \left((\mu_{\neq})^2 S_{ij}^{(1)} + (\mu_{\sim})^2 S_{ij}^{(2)} \right) \right]. \end{aligned} \quad (\text{A.4})$$

Arguing as in Step 2 and Step 3 of the proof of Proposition 4.2 of CHEVALLIER and OST (2024), one can show that there exists a positive constant K , independent of N , such that

$$\begin{aligned} \mathbb{E}_{p,q,\beta} \left[\max_{i \neq j} \left| S_{ij}^{(r)} - \frac{1}{2} (2\beta - 1)^2 m (1 - m) \left(\mathbf{1}_{\{i,j \in C_r\}} p^2 + \mathbf{1}_{\{i,j \notin C_r\}} q^2 + \mathbf{1}_{\{i \neq j\}} pq \right) \right| \right] \\ \leq K \sqrt{\frac{\log(N)}{N}}, \end{aligned} \quad (\text{A.5})$$

for $r \in \{1, 2\}$. As a consequence, defining the following N^2 -dimensional vector

$$\varepsilon_1 = L \operatorname{vec}(\operatorname{diag}(v)) - \frac{2m(1-m)}{N} \left((\mathcal{G}^2)_{11} a_{\sim} + (\mathcal{G}^2)_{12} a_{\neq} \right), \quad (\text{A.6})$$

one obtains, combining (A.4) and (A.5) together with the triangle inequality, that

$$\mathbb{E}_{p,q,\beta} [\|\varepsilon_1\|_{\infty}] \leq K \sqrt{\frac{\log(N)}{N^3}}. \quad (\text{A.7})$$

In what follows, we deal with the remaining terms $L^k \operatorname{vec}(\operatorname{diag}(v)), k \geq 2$. To that end, let us define the following N^2 -dimensional vectors

$$\begin{aligned} \varepsilon_2 &= L a_{\sim} - \left((\mathcal{G}^2)_{11} a_{\sim} + (\mathcal{G}^2)_{12} a_{\neq} \right), \\ \varepsilon_3 &= L a_{\neq} - \left((\mathcal{G}^2)_{21} a_{\sim} + (\mathcal{G}^2)_{22} a_{\neq} \right). \end{aligned} \quad (\text{A.8})$$

For any $i, j \in [N]$, observe that $(L a_{\sim})_{ij} = \mathbf{1}_{\{i \neq j\}} \sum_{(k,\ell) \in [N]^2: k \neq \ell, k \sim \ell} A_{ki} A_{\ell j}$. Similarly

as before, introducing the random variables

$$Z_{ij}^{(r)} = \frac{1}{N^2} \sum_{(k,\ell) \in C_r^2: k \neq \ell} \theta_{ki} \theta_{\ell j} \eta_{ki} \eta_{\ell j}, \quad i, j \in [N], \quad r \in \{1, 2\},$$

and using the definition of the matrix A , we can write

$$\begin{aligned} (La_{\sim})_{ij} &= \mathbb{1}_{\{i \neq j\}} \left[\mathbb{1}_{\{i \neq j\}} \mu_{\sim} \mu_{\neq} (Z_{ij}^{(1)} + Z_{ij}^{(2)}) \right. \\ &\quad \left. + \mathbb{1}_{\{i, j \in C_1\}} \left((\mu_{\sim})^2 Z_{ij}^{(1)} + (\mu_{\neq})^2 Z_{ij}^{(2)} \right) + \mathbb{1}_{\{i, j \in C_2\}} \left((\mu_{\neq})^2 Z_{ij}^{(1)} + (\mu_{\sim})^2 Z_{ij}^{(2)} \right) \right]. \end{aligned} \quad (\text{A.9})$$

Proceeding as in Lemma 8.1 of CHEVALLIER and OST (2024), we can show that

$$\mathbb{E}_{p,q,\beta} \left[\max_{i \neq j} \left| Z_{ij}^{(r)} - \frac{(2\beta - 1)^2}{4} (\mathbb{1}_{\{i, j \in C_r\}} p^2 + \mathbb{1}_{\{i, j \notin C_r\}} q^2 + \mathbb{1}_{\{i \neq j\}} pq) \right| \right] \leq K \sqrt{\frac{\log(N)}{N}}, \quad (\text{A.10})$$

for $r \in \{1, 2\}$. As a consequence, using (A.9), (A.10) and the triangle inequality, we obtain that

$$\mathbb{E}_{p,q,\beta} [\|\varepsilon_2\|_{\infty}] \leq K \sqrt{\frac{\log(N)}{N}}, \quad (\text{A.11})$$

for some constant K not depending on N . From similar arguments, we can also show that

$$\mathbb{E}_{p,q,\beta} [\|\varepsilon_3\|_{\infty}] \leq K \sqrt{\frac{\log(N)}{N}}. \quad (\text{A.12})$$

Using (A.6) and (A.8), it can be shown that for all $k \geq 2$, it holds that

$$\begin{aligned} L^k \text{vec}(\text{diag}(v)) &= \frac{2m(1-m)}{N} \left((\mathcal{G}^{2k})_{11} a_{\sim} + (\mathcal{G}^{2k})_{12} a_{\neq} \right. \\ &\quad \left. + \sum_{\ell=1}^{k-1} (\mathcal{G}^{2\ell})_{11} L^{(k-1)-\ell} \varepsilon_2 + \sum_{\ell=1}^{k-1} (\mathcal{G}^{2\ell})_{12} L^{(k-1)-\ell} \varepsilon_3 \right) + L^{k-1} \varepsilon_1. \end{aligned} \quad (\text{A.13})$$

Setting $\text{Err}_k = L^k \text{vec}(\text{diag}(v)) - \frac{2m(1-m)}{N} ((\mathcal{G}^{2k})_{11} a_{\sim} + (\mathcal{G}^{2k})_{12} a_{\neq})$, the identity (A.13) implies that for all $k \geq 2$,

$$\begin{aligned} \|\text{Err}_k\|_{\infty} &\leq \frac{2m(1-m)}{N} \left(\left\| \sum_{\ell=1}^{k-1} (\mathcal{G}^{2\ell})_{11} L^{(k-1)-\ell} \varepsilon_2 \right\|_{\infty} + \right. \\ &\quad \left. + \left\| \sum_{\ell=1}^{k-1} (\mathcal{G}^{2\ell})_{12} L^{(k-1)-\ell} \varepsilon_3 \right\|_{\infty} \right) + \|L^{k-1} \varepsilon_1\|_{\infty}. \end{aligned}$$

Now, using that $|(\mathcal{G}^{2\ell})_{11}| \leq \|\mathcal{G}^{2\ell}\|_{\infty}$ (similarly for $|(\mathcal{G}^{2\ell})_{12}|$) and the fact that the norm $\|\cdot\|_{\infty}$ is sub-multiplicative we obtain for each $r \in \{1, 2\}$,

$$\left\| \sum_{\ell=1}^{k-1} (\mathcal{G}^{2\ell})_{1r} L^{(k-1)-\ell} \varepsilon_{1+r} \right\|_{\infty} \leq \left\| \varepsilon_{1+r} \right\|_{\infty} \sum_{\ell=1}^{k-1} \max\{\|\mathcal{G}^2\|_{\infty}, \|L\|_{\infty}\}^k,$$

and also that $\|L^{(k-1)-\ell}\|_{\infty} \|\varepsilon_3\|_{\infty} \leq \|L\|_{\infty}^{k-1} \|\varepsilon_1\|_{\infty}$. Combining the above estimates, we obtain that

$$\begin{aligned} \|\text{Err}_k\|_{\infty} &\leq \frac{2m(1-m)}{N} (\|\varepsilon_2\|_{\infty} + \|\varepsilon_3\|_{\infty}) \sum_{\ell=1}^{k-1} \max\{\|\mathcal{G}^2\|_{\infty}, \|L\|_{\infty}\}^k + \|L\|_{\infty}^{k-1} \|\varepsilon_1\|_{\infty} \\ &\leq \frac{b_k}{N} (\|\varepsilon_2\|_{\infty} + \|\varepsilon_3\|_{\infty}) + \|L\|_{\infty}^{k-1} \|\varepsilon_1\|_{\infty}, \end{aligned}$$

where $b_k = 2m(1-m)(k-1) \max\{\|\mathcal{G}^2\|_{\infty}, \|L\|_{\infty}\}^k$ is a constant independent of N , that is summable in k , since $\|L\|_{\infty} < 1$ and $\|\mathcal{G}^2\|_{\infty} < 1$. Thus, it holds that

$$\left\| \sum_{k=2}^{\infty} \text{Err}_k \right\|_{\infty} \leq \sum_{k=1}^{\infty} \|\text{Err}_k\|_{\infty} \leq \frac{C}{N} (\|\varepsilon_2\|_{\infty} + \|\varepsilon_3\|_{\infty}) + \hat{C} \|\varepsilon_1\|_{\infty},$$

where C and \hat{C} are constants independent of N . Using (A.7), (A.11) and (A.12), it then follows from the above inequality that

$$\mathbb{E}_{p,q,\beta} \left[\left\| \sum_{k=1}^{\infty} \text{Err}_k \right\|_{\infty} \right] \leq K \sqrt{\frac{\log(N)}{N^3}}.$$

The proof is then complete by observing that, since $\|\mathcal{G}^2\|_{\infty} < 1$, it holds that $\sum_{k=1}^{\infty} (\mathcal{G}^{2k})_{11} = (\sum_{k=1}^{\infty} \mathcal{G}^{2k})_{11} = g_{\sim}$ and similarly $\sum_{k=1}^{\infty} (\mathcal{G}^{2k})_{12} = (\sum_{k=1}^{\infty} \mathcal{G}^{2k})_{12} = g_{\not\sim}$. \square